Anomalous diffusion of a tagged monomer with absorbing boundaries

Thesis submitted as part of the requirements for the degree of
Master of Science (M.Sc.) in Physics at Tel Aviv University
School of Physics and Astronomy

by

Assaf Amitai

The work was carried out under the supervision of
Professor Yacov Kantor

January 2009

Acknowledgments

I wish to thank my supervisor Yacov Kantor for his dedicated guidance.

I am thankful to Hemi Gutman and to all the people in his lab for their moral support.

I dedicate this work to my parents and to my grandmother.

Contents

Appendix:

Abstract

We consider the dynamics of a single ("tagged") monomer that belongs to a long polymer chain in dilute solution. At times shorter than the relaxation time of the entire polymer, the tagged monomer performs anomalous diffusion, where its mean square displacement scales with time t as t^{α}, with $\alpha < 1$. The value of α depends on the intermonomer potentials, as well as on velocity-dependent interactions between the monomers. For a non-self-interacting ("ideal") polymer without velocity-dependent forces $\alpha = 1/2$. Our model generalize anomalous diffusion of the tagged monomer to give any subdiffusion exponent ($0 < \alpha < 1$).

The dynamics of a polymer is frequently described in the Rouse (Fourier) space by Langevin equations governing the evolution of the different modes X_q. We show that by modifying the q-dependence of the noise correlation functions (and friction coefficients) in the dynamical equations, we can alter the value of α. Our dynamical model approximately corresponds to the introduction of velocity-dependent interactions that decay as a power-law of the separation between monomers ($1/r^{\chi}$), and lead to anomalous diffusion of the tagged monomer in an ideal polymer with $\alpha = 2/(2+\chi)$.

We employ our model to study the behavior of a tagged monomer in the presence of one and two absorbing boundaries, as the anomalous diffusion exponent is varied. We demonstrate the differences and similarities between this process and the process described by the fractional diffusion equation. We show that the mean time for absorption is finite in the presence of two absorbing boundaries, and that the probability distribution function of the tagged monomer decays as a power law near the boundaries.

Some aspects of the diffusion of a tagged monomer in the presence of two absorbing boundaries are analogous to the translocation of a polymer through a membrane pore. We compare the translocation of a polymer on a 2D lattice with our model, and find many qualitative similarities, as well as some quantitative differences.

Chapter 1

Introduction

Normal diffusion processes are characterized by the linear dependence of the mean square displacement of the stochastic variable $\boldsymbol{x}$ in time t, $\langle(\Delta\boldsymbol{x})^2\rangle = 2dDt$, where D is the diffusion coefficient and d is the dimensionality. Anomalous diffusion processes are usually characterized by a mean square displacement that is not linear in time but behaves as

$$\langle(\Delta\boldsymbol{x})^2\rangle = 2dK_\alpha t^\alpha, \tag{1.1}$$

where K_α is a modified diffusion coefficient with dimensions of cm^2 s$^{-\alpha}$. The exponent α determines whether the process is called superdiffusion for $\alpha > 1$ (faster than normal diffusion) or subdiffusion for $\alpha < 1$ (slower than normal diffusion) [1].

There are many processes in which this form of diffusion is observed. In physical systems, examples include the transport of charge carriers in a semiconductor [2], turbulent flow [3] and dynamics of polymeric systems [4]. In biological systems, instances include the diffusion of proteins along the DNA strands [5, 6], the motion of vesicles along filament, the foraging behavior of a number of animal species [7, 8] and the translocation of polymers through a pore in a membrane [9].

In this work, we investigate the dynamics of polymers. Specifically, we concentrate on the diffusion of a single monomer in a polymer, which we call a *tagged* monomer. The diffusion of a tagged monomer is known to be anomalous (subdiffusion) [10, 11]. We developed a model, which extends the dynamics of the tagged monomer to include any subdiffusion exponent and study the behavior in the presence of absorbing boundaries. We compare our results to those of other anomalous diffusion models. Our model is not only of interest as a polymeric system for the investigation of anomalous diffusion but

there is also a similarity between the diffusion of the tagged monomer and the translocation of a polymer through a pore in the membrane. The latter process has been the focus of intense interest and debate in recent years. We discuss the applicability of our model to the translocation process.

Chapter 2

Theoretical review

In this chapter, we review the equilibrium and dynamical properties of a single polymer chain (detailed discussions can be found in [4] and in [12]). These properties of the polymer give the basis for the model detailed in chapter 3.

2.1 Single polymer chain

Macromolecules play a significant role in constructing the world around us. They constitute a large portion of biological systems and they are also commonplace in chemical processes. A polymer is a macromolecule composed of a sequence of recurring structural units called *monomers*. When the monomers are alike it is called a homopolymer. Monomers can be connected one to another to form a long linear polymer chain, or they can be cross linked to create a polymer network. Since the mid-20th century, much effort has gone into constructing physical models describing the behavior of polymers. One can go quite far with very simple models. We begin by describing a model for a linear polymer chain, where each monomer is connected to only two adjacent monomers.

Let us consider a random process in which a particle moves on a lattice. In figure 2.1 we illustrate such a process. The particle moved on a two dimensional lattice, and at each step had a choice of four points as its next position. Thus, each of the choices had a probability of $1/4$. The process was stopped after 100 steps.

We can make the analogy between the random process and a single polymer chain. The position of the particle after n steps is taken to be the position of the n-th monomer, where $n = 0, 1, ...N$. In this way the particle dynamics of N steps is mapped to one possible conformation of a polymer of $N + 1$ monomers. The result of the random walk

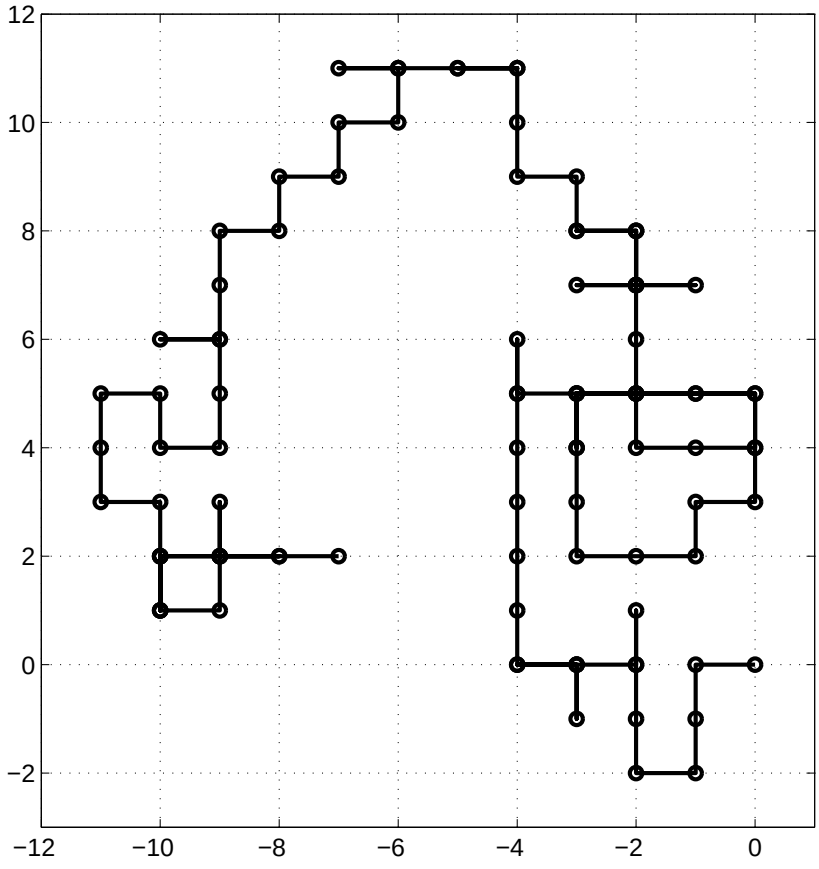

Figure 2.1: Illustration of a random walk of 100 steps on a square 2D lattice.

process is a snapshot of the corresponding polymer's conformation. In our random walk model, we allowed the particle to return to the same point. In analogy, the polymer is allowed to cross itself and is therefore called an *ideal* or *phantom* polymer.

The distance between the first and last monomer is called the end-to-end vector $\boldsymbol{R}_{ee}$. It is a measure of the size and compactness of the polymer. $\boldsymbol{R}_{ee}$ is given by the sum of N steps $\boldsymbol{b}_n$

$$\boldsymbol{R}_{ee} = \sum_{n=1}^{N} \boldsymbol{b}_n. \tag{2.1}$$

When each point of the lattice has z neighbors, each of the steps $\boldsymbol{b}_i$ has z possibilities and is independent from the others. From the definition of $\boldsymbol{R}_{ee}$ one can show that it has the following properties:

1. The average square end-to-end vector is linear in N:

$$\langle \boldsymbol{R}_{ee}^2 \rangle = Nb^2. \tag{2.2}$$

2. For long walks ($N \gg 1$) the shape of the distribution function for $\boldsymbol{R}_{ee}$ is Gaussian

$$p\left(\boldsymbol{R}_{ee}\right) = \left[\frac{d}{2\pi N b^2}\right]^{d/2} \exp\left(-d\ \boldsymbol{R}_{ee}^2 / 2Nb^2\right), \tag{2.3}$$

   where d is the dimensionality of the lattice.

The polymer has many possible conformations. Because there are no interactions between the monomers, all conformations are of the same energy and have equal probabilities. In this simple case, the entropy is the only non-trivial contribution to the free energy of the chain. The entropy S is the logarithm of the number of states and can be derived from equation 2.3:

$$S\left(\boldsymbol{R}_{ee}\right) = S\left(0\right) - \frac{k_B\ d\ \boldsymbol{R}_{ee}^2}{2Nb^2}. \tag{2.4}$$

Another important model, in which the polymer is not restricted to a lattice is the *"freely joined chain"*. In this model, the polymer consists of $(N+1)$ point particles connected to each other with bonds of fixed length b and able to take any orientation in space. As in the "lattice version", the average square of the end-to-end vector is linear in N. It is useful to define the *radius of gyration* which is a more robust measure of the

polymer's size than R_{ee}^2 as it includes the position of all monomers:

$$R_g^2 = \frac{1}{N+1}\sum_{i=0}^{N}\left(\boldsymbol{R_i} - \boldsymbol{R}_{\text{cm}}\right)^2, \tag{2.5}$$

where $\boldsymbol{R_i}$ is the position of particle i and $\boldsymbol{R}_{\text{cm}} = \frac{1}{N+1}\sum_{i=0}^{N}\boldsymbol{R_i}$ is the center mass position. For long chains it gives [4]

$$R_g^2 \approx \frac{Nb^2}{6}. \tag{2.6}$$

Furthermore, it was found that restricting the successive bond orientation still leads to the linear dependence R_g^2 in N, with only a change of a constant, i.e. b is replaced with an effective bond length $\bar{b}^2 \equiv \langle b^2 \rangle$ and N is replaced with an effective chain length.

So far we gave examples of discrete models of polymers. In the large N limit, the previous models gave a Gaussian distribution of the end-to-end vector. We are motivated to define the *Gaussian chain* model in which the bond length $\boldsymbol{R}_n - \boldsymbol{R}_{n-1}$ has the Gaussian distribution with variance of b^2. This chain can be represented by a mechanical model: $N+1$ beads connected by harmonic springs. We can define an effective Hamiltonian

$$H = \frac{d\, k_B T}{2b^2}\sum_{n=1}^{N}\left(\boldsymbol{R}_n - \boldsymbol{R}_{n-1}\right)^2, \tag{2.7}$$

which at equilibrium, gives us the probability distribution of the chain:

$$\psi(\{\boldsymbol{r}_n\}) = \left[\frac{d}{2\pi b^2}\right]^{dN/2}\exp\left(-\sum_{n=1}^{N}\frac{d\ \left(\boldsymbol{R}_n - \boldsymbol{R}_{n-1}\right)^2}{2b^2}\right), \tag{2.8}$$

which is just the normalized Boltzmann factor for H.

It can be shown that, in this model, the distance distribution between any two beads m and n is also Gaussian, given by

$$\phi(\boldsymbol{R}_n - \boldsymbol{R}_m) = \left[\frac{d}{2\pi b^2\,|n-m|}\right]^{d/2}\exp\left(-\frac{d\ \left(\boldsymbol{R}_n - \boldsymbol{R}_m\right)^2}{2b^2\,|n-m|}\right), \tag{2.9}$$

while the mean square separation between them is

$$\left\langle \left(\boldsymbol{R}_n - \boldsymbol{R}_m\right)^2 \right\rangle = |n-m|\, b^2. \tag{2.10}$$

The monomer index n is often regarded as a continuous variable:

$$\Pi(\{\boldsymbol{R}_n\}) = \text{const}\ \exp\left[\int_0^N \frac{d}{2b^2}\ \left(\frac{\partial \boldsymbol{R}_n}{\partial n}\right)^2 dn\right]. \tag{2.11}$$

In the models we have discussed so far, the monomers interacted only with their neighbors along the chain. In real polymers, every two monomers that come close interact. Since each monomer has a certain volume, two monomers cannot occupy the same position in space. Therefore, a repulsion interaction occurs beyond a certain proximity, known as *excluded volume interaction*. In one dimension, the effect of excluded volume interaction is to stretch the polymer completely, as it cannot overlap itself. In higher dimensions, the effect of the interaction leads to a significant swelling of the polymer size. The excluded volume effect was first considered by Kuhn and Flory [13, 14]. They established that this interaction changes the equilibrium properties of the polymer. For ideal polymers we had $\langle \boldsymbol{R}_{ee}^2 \rangle \approx N$; but, with the addition of the interaction

$$\langle \boldsymbol{R}_{ee}^2 \rangle \approx N^{2\nu}, \tag{2.12}$$

where the exponent ν depends only on the dimensionality: $\nu = 3/4$ for $d = 2$ and $\nu \approx 0.588$ for $d = 3$ [4].

2.2 Dynamical properties of polymers

The equilibrium properties of a polymer are described by microscopic random walk approaches, where every step accounts for a monomer's location. The dynamics of a polymer can be described using the Fokker-Planck equation for many bodies [15]. In this treatment, the probability distribution of the monomers in space and their change in time are calculated. A different approach taken by Rouse [16] is to use the Langevin equation, where instead of representing the monomer by its probability distribution, it is treated as a particle. The statistical nature of the process comes from an external random force which affects the monomers. As the coefficients in the Fokker-Planck equation depend on the averages of the Langevin equation, all average properties of the polymer calculated with the two methods are equal.

The Langevin equation is used to describe many processes where a system is affected by a random noise, such as diffusing particles and current fluctuations in an electrical circuit, among others [17]. In its simplest form, the Langevin equation describes the motion of a particle of mass m in a fluctuating environment subjected to a randomly fluctuating force and to a friction force. The friction force, to the first order, depends on the particle

velocity $\boldsymbol{v}$ and a constant ζ, $\boldsymbol{F} = -\zeta \boldsymbol{v}$. The friction constant ζ, depends on the particle size and the viscosity of the fluid. The random force and the friction force has a similar origin. In a solute, the solvent particles diffuse randomly, colliding with each other and with the particle, and create in this way a random force. When the particle moves in a certain direction, more solvent particles would collide with it from that direction, than from the opposite one, which can be described by an effective friction force. From the equipartition theorem, we know that at any time the mean energy of the particle is $\frac{1}{2}m\langle \boldsymbol{v}^2 \rangle = \frac{3}{2}k_B T$ (in three dimensions). The fluctuating force gives us the correct thermal energy. Under these conditions, the Newtonian equation of motion is:

$$m\frac{d\boldsymbol{v}}{dt} = -\zeta \boldsymbol{v} + \boldsymbol{f}\left(t\right) - \frac{\partial U}{\partial \boldsymbol{x}}, \tag{2.13}$$

where U is the potential energy and $\boldsymbol{f}$ is the fluctuating force whose properties are given by its averages. The average over the whole ensemble is zero as there is no preferred direction of motion:

$$\left\langle f_\alpha\left(t\right)\right\rangle = 0. \tag{2.14}$$

We assume that the collisions of the fluid particles are independent of one another after a certain amount of time τ_0. This time is usually much smaller than the relaxation time $\tau = m/\zeta$ of the particle. Therefore, we may take the limit of $\tau_0 \to 0$. The correlation of the random force is thus given by

$$\left\langle f_\alpha\left(t\right) f_\beta\left(t'\right)\right\rangle = 2\zeta k_B T \delta_{\alpha,\beta}\delta\left(t - t'\right). \tag{2.15}$$

In the over-damped case of the Langevin equation, the damping term dominates the dynamics and is much larger than the inertia term. Thus, the inertia part in equation (2.13) can be neglected.

We can now write the Langevin equation for the position $\boldsymbol{R}_n$ of the n-th monomer with the influence of the potential given by equation (2.7)

$$\zeta\frac{d\boldsymbol{R}_n}{dt} = -\kappa(2\boldsymbol{R}_n - \boldsymbol{R}_{n+1} - \boldsymbol{R}_{n-1}) + \boldsymbol{f}_n, \quad \text{for } 1 < n < N. \tag{2.16}$$

And for the end monomers

$$\zeta\frac{d\boldsymbol{R}_1}{dt} = -\kappa(\boldsymbol{R}_1 - \boldsymbol{R}_2) + \boldsymbol{f}_1 \tag{2.17a}$$

$$\zeta\frac{d\boldsymbol{R}_N}{dt} = -\kappa(\boldsymbol{R}_N - \boldsymbol{R}_{N-1}) + \boldsymbol{f}_N, \tag{2.17b}$$

where $\kappa = 3k_BT/b^2$ in $d = 3$. The random noise $\boldsymbol{f}_n$ acting on monomer n is independent of the noise acting on monomer m, and is also uncorrelated in time. The random noise can be characterized by its first and second moments:

$$\langle f_{n,\alpha} \rangle = 0 \tag{2.18}$$

$$\langle f_{n,\alpha}(t)\, f_{m,\beta}(t') \rangle = 2\zeta k_B T \delta_{n,m} \delta_{\alpha,\beta} \delta(t - t'), \tag{2.19}$$

where α and β are the spatial unit vectors.

The problem would be easier to solve if the dynamical equations (2.17) for the end monomers were similar to those of the other monomers (equation (2.16)). If we define two additional hypothetical monomer $\boldsymbol{R}_0$ and $\boldsymbol{R}_{N+1}$, and set a condition on them so that $\boldsymbol{R}_0 = \boldsymbol{R}_1$ and $\boldsymbol{R}_{N+1} = \boldsymbol{R}_N$, we can see that indeed, all monomers follow the same dynamical equation (2.16). The Rouse model gives us N coupled equations, where the motion of every monomer depends on that of the adjacent monomers and the external noise. Since the equations are similar to that of coupled oscillators, we can use a standard method to solve them by Fourier transforming from monomer coordinates $\boldsymbol{R}_n$ to normal coordinates (Rouse modes) $\boldsymbol{X}_p$. The transformation is given by the discrete cosine transform which fulfills the condition on the end monomers:

$$\boldsymbol{X}_p = \frac{1}{N} \sum_{n=1}^{N} \boldsymbol{R}_n \cos\left(n - \frac{1}{2}\right) \frac{p\pi}{N} \tag{2.20a}$$

$$\boldsymbol{R}_n = \boldsymbol{X}_0 + 2 \sum_{p=1}^{N-1} \boldsymbol{X}_p \cos\left(n - \frac{1}{2}\right) \frac{p\pi}{N}, \tag{2.20b}$$

The properties of the transformation are described in appendix A.1.

The location of a monomer $\boldsymbol{R}_n$ depends on each of the $N - 1$ (internal) modes and the movement of the center of mass $\boldsymbol{X}_0$. In terms of Rouse modes, the motion is described by N independent equations

$$\zeta_p \frac{d\boldsymbol{X}_p}{dt} = -\kappa_p \boldsymbol{X}_p + \boldsymbol{W}_p, \tag{2.21}$$

where

$$\kappa_p = 8N\kappa \sin^2\left(\frac{p\pi}{2N}\right), \tag{2.22}$$

and the mode dependent friction coefficient

$$\begin{aligned} \zeta_p &= 2N\zeta \quad (p = 1, 2, ...), \\ \zeta_0 &= N\zeta, \end{aligned} \tag{2.23}$$

while $\boldsymbol{W}_p$ is the noise with corresponding mean and correlation

$$\langle W_{p,\alpha}(t)\rangle = 0, \tag{2.24a}$$

$$\langle W_{p,\alpha}(t)\, W_{p',\beta}(t')\rangle = 2k_B T\zeta_p \delta_{p,p'}\delta_{\alpha,\beta}\delta(t-t'). \tag{2.24b}$$

The exact derivation of the equation is detailed in appendix A.2. Equation (2.21) is similar to the equation of a particle in an harmonic potential with noise. It can be solved analytically (appendix A.3). The mean of the mode amplitude decays exponentially to zero as $\langle \boldsymbol{X}_p(t)\rangle = \boldsymbol{X}_p(t=0)\exp(-t/\tau_p)$ for $p \neq 0$, and $\tau_p = \frac{\zeta_p}{\kappa_p}$ is the characteristic relaxation time of mode p. The mean square deviation of the mode (for $p \neq 0$) is given by

$$\langle (\boldsymbol{X}_p(t) - \langle \boldsymbol{X}_p(t)\rangle)^2\rangle = \frac{k_B T}{\kappa_p}[1-\exp(-2t/\tau_p)]. \tag{2.25}$$

The center of mass $\boldsymbol{X}_0$ undergoes normal diffusion with a diffusion coefficient of $D_{\text{cm}} = k_B T/\zeta N$.

Although the Rouse model is very elegant and gives many important results, it proves problematic when we compare it to experiments. Experimentally, when the center mass diffusion is measured as a function of the polymer's length N, it scales as $D_{\text{cm}} \propto N^{-1/2}$ [12], while the model predicts $D_{\text{cm}} \propto N^{-1}$. This disparity comes from the neglect of hydrodynamical interactions.

In 1956, Zimm came up with a new model [18] which accounts for hydrodynamical interactions. Suppose we have Brownian particles suspended in a solution, interacting with each other. The motion of a certain particle causes the fluid around it to move, thereby creating a force which affects the motion of the other particles. Their motion in turn, affects that of the first particle. This solvent-mediated action is called hydrodynamical interaction. In the Rouse model, the velocity of a monomer n depended only on the forces acting on it $\boldsymbol{v}_n = \frac{1}{\zeta}\boldsymbol{F}_n$. Now, as a result of the hydrodynamical interactions, it depends on all monomers. With the addition of the interaction, the velocity of a monomer n is to the first order, a linear combination of the forces acting on it from all the other monomers $\boldsymbol{v}_n = \sum_m \boldsymbol{H}_{nm}\boldsymbol{F}_m$. The mobility matrix $\boldsymbol{H}_{nm}$ couples the motion of all monomers. It has the form:

$$\boldsymbol{H}_{nm} = \begin{cases} \boldsymbol{I}/\zeta & n = m \\ \frac{1}{8\pi\eta|\boldsymbol{r}_{nm}|}\left[\hat{\boldsymbol{r}}_{nm}\hat{\boldsymbol{r}}_{nm} + \boldsymbol{I}\right] & n \neq m, \end{cases} \tag{2.26}$$

where η is the viscosity, $\boldsymbol{r}_{nm} = \boldsymbol{R}_n - \boldsymbol{R}_m$ and $\hat{\boldsymbol{r}}_{nm}$ is a unit vector in the direction of $\boldsymbol{r}_{nm}$. $\boldsymbol{H}_{nm}$ is called the Oseen tensor for hydrodynamical interactions [12].

We can generalize equation (2.16) to include the influence of velocities of different monomers to get

$$\frac{\partial \boldsymbol{R}_n(t)}{\partial t} = \sum_m \boldsymbol{H}_{nm} \left(-\frac{\partial U}{\partial \boldsymbol{R}_m} + \boldsymbol{f}_m(t) \right). \tag{2.27}$$

Trying to solve the problem explicitly is hard, as we would have to solve N nonlinear coupled equations. Rather than solving equation (2.27) explicitly, Zimm suggested replacing the mobility tensor $\boldsymbol{H}_{nm}$ with its average over all polymer configuration. Assuming an equilibrium condition, $\langle \boldsymbol{H}_{nm} \rangle$ is calculated using the monomers probability distribution (2.9). (This procedure is called preaveraging.) After the preaveraging and transformation to Rouse modes, the equations for the different modes decouple (in the limit of $N \gg 1$) and obey equation (2.21) with modified friction coefficients

$$\begin{aligned} \zeta_p &= \left(12\pi^3\right)^{1/2} \eta b \left(Np\right)^{1/2} \quad (p = 1, 2, ...) \\ \zeta_0 &= \frac{3}{8} \left(6\pi^3\right)^{1/2} \eta b N^{1/2}. \end{aligned} \tag{2.28}$$

The center mass of the polymer diffuse normally with a diffusion coefficient

$$D_{\text{cm}} = \frac{k_B T}{\zeta_0} \propto N^{-1/2} \tag{2.29}$$

and each of the modes have the characteristic relaxation time of

$$\tau_p = \zeta_p / \kappa_p \propto p^{-3/2}. \tag{2.30}$$

This result for the center mass diffusion coefficient agrees with the experimental results discussed previously.

The hydrodynamical interaction changes the dynamics of the polymer while its equilibrium properties are not modified. For this reason, the value of κ_p remains the same. Introduction of self-avoiding interactions, however, would change them thorough a modification of κ_p [12].

In the Zimm model, contrary to Rouse's, the interactions are non-local. This is the key difference between them. The interactions between monomers velocities lead to different p dependence of the relaxation times of the modes. In the following chapters, we show how, control of the p-dependence of τ_p can create arbitrary subdiffusion exponents.

2.3 Anomalous diffusion

2.3.1 Review of models

Anomalous diffusion occurs in many physical and biological systems. These processes are characterized by the mean square displacement of the stochastic variable increase with time t as t^α, where processes with $\alpha > 1$ are called superdiffusion and for $\alpha < 1$ they are called subdiffusion. The first report of anomalous diffusion was in 1926, in Richardson's study of turbulent superdiffusion with $\alpha = 3$ (processes with $\alpha > 2$ are known as ballistic) [3]. Later, a study of dispersive transport of amorphous semiconductors by Scher and Montroll [2] showed that charge carrier exhibits subdiffusion. Others showed that motion of particles in percolative systems [19] and porous media [20] also exhibit subdiffusion. Superdiffusion, however, is observed in collective diffusion on solid surfaces [21] and in bulk-surface exchange controlled dynamics in porous glasses [22].

Polymeric systems are a rich source of anomalous behavior. The motion of the center mass of a polymer in a dense polymer solution (known as reptation) shows subdiffusion with $\alpha = 1/2$ [23]. If we observe the motion of a specific (*tagged*) monomer in a single ideal polymer chain performing Rouse dynamics, we find that it exhibits subdiffusion with $\alpha = 1/2$ [10, 11]. The latter motion which is closely related to the subject of this study is anomalous, not due to an embedded anomaly in the surroundings, but because of the monomers collective motion.

Within a biological cell, micelles traveling by motor proteins were shown to perform superdiffusion with an exponent of $\alpha = 3/2$. DNA-binding proteins diffusing along a double stranded DNA can perform subdiffusion [5]. In other cases, a protein can detach itself from the chain and connect to another segment nearby in three dimensions but far along the chain. This motion produces superdiffusion behaving like Lévy flights [6]. The passage of polymers through a membrane pore, a process known as translocation, was shown to be anomalous with a subdiffusion exponent (we will review the translocation process in detail in chapter 5).

Animals searching for food sample their surroundings and, if nothing of interest is found, they move to a remote location. While trajectories of normal diffusion tend to be redundant, as they cross themselves repeatedly and sample the same space several

times, Lévy flight's trajectories spread on more space by taking the occasional large jump. Apparently, such a strategy is better suited for animal resource search patterns. Analysis of the traveling and searching trajectories of several animal species, such as the flight of the albatross [7] and the movement of bacteria [24] and spider monkeys [8], have revealed that they perform Lévy flights with $\alpha \approx 1.7$ [8].

There are several physical and mathematical models that produce anomalous diffusion. We will review some of them here, and later compare their results to those produced by our model. Detailed discussion can be found in [1, 25].

Subdiffusion usually occurs in systems with strong memory effects. The most basic formalism to describe this is a generalization of Brownian motion called *continuous time random walk* (CTRW). Instead of a normal diffusion discrete model where a particle moves a fixed distance every step, one can define a diffusion model such that both the waiting time between steps and the length of the step are taken from probability distributions $\psi(t)$ and $\lambda(x)$ respectively. Their corresponding mean time and variance are given by $T = \int_0^\infty dt\psi(t)\, t$ and $\Sigma^2 = \int_{-\infty}^\infty dx\lambda(x)\, x^2$, which can be either finite or diverging. Taking a Poissonian distribution for the waiting times and a Gaussian distribution for the steps length reproduces, in the long-time limit, the regular Brownian dynamics. Actually, every process where T and Σ are finite will reproduce this dynamics.

When the waiting time distribution has a long-tailed asymptotic behavior $\psi(t) \approx A_\alpha (\tau/t)^{1+\alpha}$, with $0 < \alpha < 1$, the mean time will diverge. This can happen, for example, when the particle is trapped for long times, as is the case in amorphous semiconductors [2]. For a Gaussian $\lambda(x)$, it can be shown [26] that the probability distribution $P(x,t)$ for this process obeys the dynamical equation:

$$\frac{\partial P}{\partial t} = {}_0D_t^{1-\alpha} K_\alpha \frac{\partial^2 P}{\partial x^2}. \tag{2.31}$$

Equation (2.31) is known as the *fractional diffusion equation* (FDE) which reduces for $\alpha = 1$ to the regular diffusion equation. ${}_0D_t^{1-\alpha}$ is the Riemann-Liouville operator which, for $0 < \alpha < 1$, is defined through the relation

$${}_0D_t^{1-\alpha} P(x,t) = \frac{1}{\Gamma(\alpha)} \frac{\partial}{\partial t} \int_0^\infty dt' \frac{P(x,t')}{(t-t')^{1-\alpha}}. \tag{2.32}$$

This is a fractional differentiation of a power q

$${}_0D_t^q t^p = \frac{\Gamma(1+p)}{\Gamma(1+p-q)} t^{p-q}, \tag{2.33}$$

which holds for any real q. Solving equation (2.31) with the initial condition $P(x,0)=\delta(x)$ and calculating the mean square displacement indeed gives us:

$$\langle x^2(t)\rangle = \frac{2K_\alpha}{\Gamma(1+\alpha)}t^\alpha. \tag{2.34}$$

For the case of diffusion in an external potential the fractional diffusion equation can be generalized to give the fractional Fokker-Planck equation (FFPE).

Many anomalous diffusion processes are described using the Lévy flights (LF) model. LF is a Markov process which has a broad jump length distribution with an asymptotic power law

$$\lambda(x) \approx \frac{\sigma^\mu}{|x^{1+\mu}|}, \tag{2.35}$$

such that the variance diverges. The trajectories of are fractals, with the fractal dimension of μ. Unlike Gaussian random walk that 'fill' the area, LFs trajectories consist of self-similar clusters, separated by long jumps. The waiting time distribution in LFs, is sharply peaked with a finite characteristic mean time τ. If we Fourier transform λ, we get a part that behaves as $|k|^\mu$, whereas in the Gaussian case, we would get $|k|^2$. The fractional derivative is sometimes defined through its Fourier transform [25]

$$\mathcal{F}\left\{\frac{d^\mu g}{d|x|^\mu}\right\} \equiv -|k|^\mu g(k), \tag{2.36}$$

where $1 \le \mu < 2$. And the Lévy process can be defined though a fractional diffusion equation

$$\frac{\partial}{\partial t}P(x,t) = K^\mu \frac{\partial^\mu}{\partial|x|^\mu}P(x,t), \tag{2.37}$$

with the generalized diffusion coefficient $K^\mu \equiv \sigma^\mu/\tau$ and $\partial^\mu/|x|^\mu$ that is called the Riesz-Feller derivative. The probability density of LF has the power-law asymptotic form of $P(x,t) \approx K^\mu t/|x|^\mu$ for $\mu < 2$. As a result of this property, the mean squared displacement diverges.

The Riesz-Feller derivative appears also in the equation for stochastically growing surfaces where the height of the surface is dynamically described by the Langevin equation [27, 28]. The equations of our model, which will be presented in the next chapter, are very similar to the equation describing the surface's height, and can be used to describe its dynamics.

The definition of the Riesz-Feller derivative is done through the Fourier space. This operator derivative is sometimes written as a fractional Laplacian operator $-(-\Delta)^{\mu/2}$

(for $\mu = 2$ the normal Laplacian is recovered). In the form of the fractional Laplacian, it is easier to describe the problem of anomalous diffusion in terms of an eigenvalue problem where the probability density function is represented by the eigenfunctions.

Another important model is *Lévy walks*, which can be described as a coupled CTRW. In this process the walker maintains a constant velocity. This is achieved by coupling the waiting time distribution and the jump length distribution. A condition on the two distributions ensures that long jumps result in long waiting times. Hence, the time of travel is proportional to the total trajectory length and the mean square displacement converges and with time, grows at a faster than linear rate.

2.3.2 Anomalous diffusion of a tagged monomer

In this work we investigate the behavior of a monomer in a long polymer chain, which we call a *tagged* monomer. The following discussion applies to any of the monomers, including the end monomers.

The description of the motion of a monomer undergoing a cooperative diffusion depends on time scale. Two important times are relevant when discussing the monomer's motion. The time is takes for the monomer to move a distance of b (the mean distance between monomers), denoted $\tau_0 \approx b^2/D_0$, and the time it takes for the polymer to diffuses its own radius of gyration $\tau_N \approx R_g^2/D_{\text{cm}} \approx b^2 N^{1+2\nu}/D_0$ (considering the Rouse model). $D_0 = k_B T/\zeta$ is the diffusion coefficient of a single monomer. At times shorter than τ_0, the monomer's motion is simple diffusion with time scaling $\langle \Delta R_n^2 \rangle \approx D_0 t$, where n is the monomer number. In this time regime, the monomer diffuses without feeling its adjacent monomers. In the long time regime $t \gg \tau_N$, the tagged monomer diffuses normally with the diffusion coefficient $\langle \Delta R_n^2 \rangle \approx \frac{D_0}{N} t$, i.e. $D_{\text{cm}} = D_0/N$. In the intermediate time regime $\tau_0 \ll t \ll \tau_N$, the monomer undergoes anomalous diffusion with $\langle \Delta R_n^2 \rangle \approx b^{2-2\alpha} (D_0 t)^{\alpha}$ [11], where $\alpha = 2\nu/(1+2\nu)$. In the case of an ideal chain ($\nu = 1/2$) we get $\alpha = 1/2$.

To observe the monomer's motion in the different time regimes, we performed a simulation in one dimension, where we followed the location of the central monomer in polymers of increasing length. The simulation method is described in the appendix B. In each simulation, we equilibrated the polymer by randomizing the initial modes amplitudes, and positioned the central monomer at the origin. The location R_c of the (central)

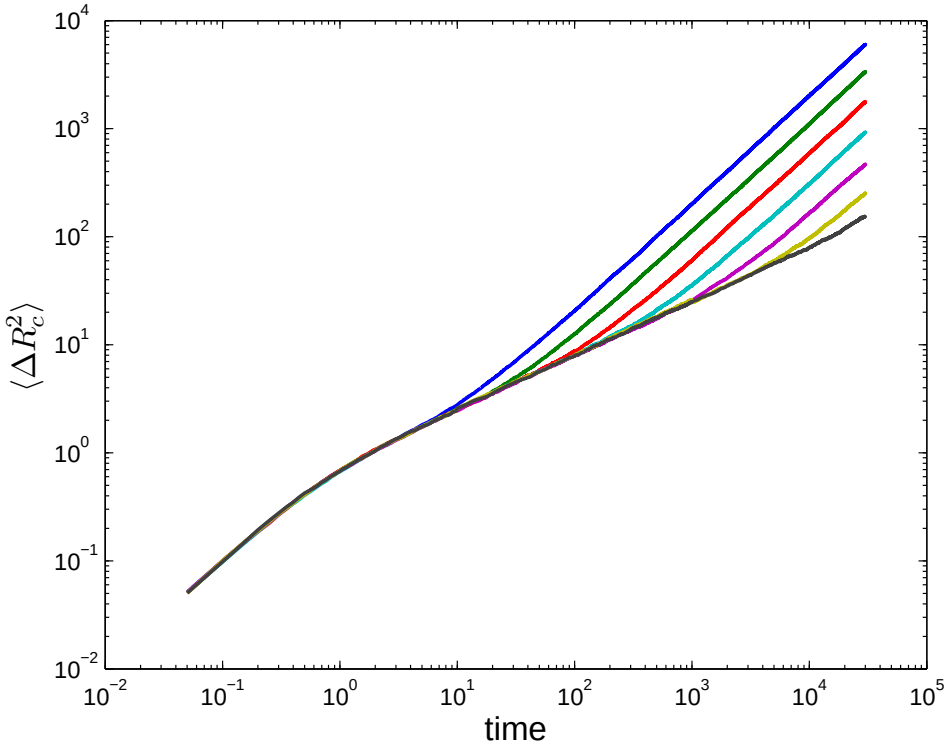

Figure 2.2: Variance of the central monomer for $N = 5, 9, 17, 33, 65, 129, 257$ (left-to-right). 10,000 runs where preformed for each polymer. The time is in units of $\tau_0 = \frac{1}{2}\frac{\zeta}{\kappa}$ while the variance is in units of b^2.

monomer $c = N/2 + 1/2$, was averaged over $10,000$ realizations and its mean square distance was found as a function of time. Figure 2.2 depicts the mean square distance of monomer c in Gaussian polymers of length $N = 5, 9, 17, 33, 65, 129, 257$. At short times the diffusion of the monomer is indeed normal for all polymers. The crossover to the anomalous regime is the same for all polymers as the monomer does not yet feel the full length of the polymer. As the polymers are Gaussian ones, the monomer diffuses with the same anomalous exponent of $\alpha = 1/2$. The difference between the curves occurs when returning to the normal diffusion regime. Because the time of the crossover is determined by the radius of gyration, the length of the anomalous regime is larger for longer polymers. In the following simulations, we usually use polymers of length $N = 257$, so that throughout the simulation time the diffusion will be anomalous.

Chapter 3

The model system

In this section, we describe the model being studied and discuss the physical motivation behind it.

3.1 Description of the model

As we noted in the previous chapter, models of anomalous dynamics are numerous. In most of them, the anomalous exponent is a free parameter of the dynamical equation. While the models' equations can later describe many physical systems, in some sense, the mathematics precedes the physics. In this chapter, we demonstrate how the physical description of a polymeric system can be used to create anomalous dynamical equations.

3.1.1 Monomer-monomer interactions

In Rouse-like models of beads and springs, the dynamics of the system is controlled by the nature of the interaction between the beads. This is evident when comparing the Rouse and Zimm models, where the first gives Rouse modes relaxation times that scale with N and p as $\tau_p \propto (N/p)^2$, while for the second they scale as $\tau_p \propto (N/p)^{3/2}$. The reason for the disparity is this: in the Rouse model the interactions are local as they are restricted to the neighbors, while in the Zimm model there are also long ranged interactions as the velocities of the distant monomers are coupled.

The equilibrium properties of the polymer are governed by the mean distance between adjacent monomers. In the Langevin equation the spring constant κ is related to the mean

inter-monomer separation b by $\kappa = 3k_BT/b^2$ (in $d = 3$). The introduction of excluded volume interactions into the dynamical equation can be done [12] by modifying the value of mode dependent spring constant κ_p. It is possible to control the dynamics of the polymer by changing κ_p, which sets the relaxation time of the modes ($\tau_p = \zeta_p/\kappa_p$). However, if we wanted to control the dynamics without changing the equilibrium properties, we would have to think of a way to change ζ_p. We could do so by coupling the velocities of the monomers. Let us introduce a nonlocal interaction between monomers' velocities that has a power law dependence on distance between them. The mobility matrix for it is given by

$$\boldsymbol{O}_{nm} = \begin{cases} \boldsymbol{I}/\zeta & n = m \\ \frac{b^\chi}{\zeta|\boldsymbol{R}_n - \boldsymbol{R}_m|^\chi}\left[\boldsymbol{I} + \hat{\boldsymbol{r}}_{nm}\hat{\boldsymbol{r}}_{nm}\right] & n \neq m, \end{cases} \tag{3.1}$$

where $\hat{\boldsymbol{r}}_{nm}$ is a unit vector in the direction of $\boldsymbol{R}_n - \boldsymbol{R}_m$. This is actually a generalization of the Zimm model (for hydrodynamical interactions $\chi = 1$).

We can write the Langevin equation (2.27) with our interaction for monomer $\boldsymbol{R}_n$:

$$\frac{\partial}{\partial t}\boldsymbol{R}_n = \sum_m \boldsymbol{O}_{nm}\left(-\frac{\partial U}{\partial \boldsymbol{R}_m} + \boldsymbol{f}_m(t)\right). \tag{3.2}$$

Equation (3.2) couples the velocities of all monomers. It is nonlinear in the monomers distance $|\boldsymbol{R}_n - \boldsymbol{R}_m|$. In order to solve it, we will linearize it first. The velocity $\boldsymbol{v}_n$ of monomer n is calculated as the summed perturbation of forces from all monomers. We assume that the effect of forces on the motion of the fluid is given by the Kirkwood-Riseman [29] approximation applied for $\boldsymbol{O}_{nm}$. In essence, $\boldsymbol{O}_{nm}$ is replaced by its average over all monomer realizations using the equilibrium monomers distance distribution function for a Gaussian polymer (2.9) (as the equilibrium properties did not change).

$$\boldsymbol{O}_{nm} \to \langle \boldsymbol{O}_{nm} \rangle = \int d\{\boldsymbol{R}_n\} \boldsymbol{O}_{nm} \Phi_{eq}\{\boldsymbol{R}_n\} \tag{3.3}$$

$$\langle \boldsymbol{O}_{nm} \rangle = \frac{A_{d,\chi}}{\zeta b\,|n-m|^{\chi/2}} \equiv h\,(n-m)\,. \tag{3.4}$$

The value of $A_{d,\chi}$ is given in appendix A.4. Note that in expression (3.4), $|n - m|$ has no exponent dependence on the dimensionality of the problem. This occurs because the averaging procedure reduces the distance between the beads to their order distance along

the polymer chain $(n-m)$. Now the Langevin equation is linear, of the form:

$$\frac{\partial}{\partial t}\boldsymbol{R}_n = \sum_m h(n-m)\left(-\frac{\partial U}{\partial \boldsymbol{R}_m} + \boldsymbol{f}_m(t)\right). \tag{3.5}$$

We can write it as a Langevin equation in terms of the Rouse normal modes $\boldsymbol{X}_p$:

$$\frac{\partial}{\partial t}\boldsymbol{X}_p = \sum_q h_{pq}\left(-\kappa_q \boldsymbol{X}_q + \boldsymbol{f}_q(t)\right), \tag{3.6}$$

where κ_p is the same as in the Gaussian case and the mobility matrix h_{pq} is the Fourier transform of the mobility matrix.

Since $h_{pq} \propto \delta_{p,q}$ in the limit of large N, equations (3.6) decouple and can be shown (see appendix A.4), to have the form of equation (2.21) with modified ζ_q. The mode-dependent mobility scales in the following way (up to a dimensionless factor)

$$h_{pq} \propto \frac{N^{1-\chi/2}}{N\zeta(q\pi)^{1-\chi/2}}\delta_{p,q}.$$

From this we calculate the friction constant

$$\zeta_q = (h_{qq})^{-1} \propto N\zeta\left(\frac{q}{N}\right)^{1-\chi/2} \tag{3.7}$$

and the friction constant for the center of mass:

$$\zeta_0 \propto \zeta N^{\chi/2}. \tag{3.8}$$

For detailed analysis of the model derivation and the model equations we refer the reader to the appendix A.4.

3.1.2 Model equations

So far we have shown that by adding a monomer-monomer interaction with a parameter χ to the Rouse model, we can arrive to the Rouse equation with modified friction coefficients, in the large N limit. Motivated by this, we now define the following model in the Rouse space. Our system is described by N Langevin equations, one for each Rouse mode ($p = 0, 1, ..., N$)

$$\zeta_p \frac{\partial}{\partial t}\boldsymbol{X}_p = -\kappa_p \boldsymbol{X}_p + \boldsymbol{W}_p(t), \tag{3.9}$$

where the noise mean and correlation are given by

$$\langle W_{p,\alpha}(t)\rangle = 0 \tag{3.10a}$$

$$\langle W_{p,\alpha}(t)\, W_{p',\beta}(t')\rangle = 2k_B T\zeta_p \delta_{p,p'}\delta_{\alpha,\beta}\delta(t-t'). \tag{3.10b}$$

The mode spring constant is defined as in the Gaussian case

$$\kappa_p = 8N\kappa \sin^2\left(\frac{p\pi}{2N}\right), \tag{3.11}$$

while

$$\zeta_p = 2C_{\chi,N} N\zeta \left(\frac{p}{N}\right)^{1-\chi/2} \tag{3.12a}$$

$$\zeta_0 = \zeta N^{\chi/2}. \tag{3.12b}$$

In the Rouse and Zimm model the slowest internal mode friction coefficient ζ_1 differs from the center mass friction coefficient by a factor of order unity. As a result, the slowest relaxation mode τ_1 is of the order of the time it takes for the polymer to diffuse its own radius of gyration. Since we wanted to adhere to that relation, we defined ζ_q with a dimensionless factor $C_{N,\chi}$ which depends on N and χ. We used our freedom in choosing C, to define it so that in the limit of very short times, a monomer diffuses with diffusion coefficient $D_0 = b^2/\tau_0$, where $\tau_0 = \frac{1}{2}\frac{\zeta}{\kappa} = \frac{\zeta b^2}{2k_B T}$. In the limit of large N, the normalization factor is reduced to $C \approx \frac{2}{\chi}$. For elaboration see appendix A.5.2.

The mode relaxation time $\tau_p = \zeta_p/\kappa_p$ has a power law dependence on the mode number p with exponent χ, where for $\chi = 2$, we get the Rouse equations for Gaussian polymer. Since each of the dynamical equations is that of a particle in harmonic potential coupled to random noise, the mean and the mean square displacement of $\boldsymbol{X}_p$ can be found analytically as described in appendix A.3.

In our derivation of the dynamical equation in the presence of the interaction between monomers' velocities we used a number of approximations - the transition from a discrete to a continuous chain and the limit of large q. It should be stressed that the shape of the operator in the real space from which equation (3.9) is derived is not that of equation (3.2). However, it gives us a very good intuitive sense of the nature of a process which will result in this kind of anomalous behavior.

Next we show how we get the anomalous exponent of the process from the model equations.

3.2 Subdiffusion of a tagged monomer

Following Kantor and Kardar [30] study of the anomalous diffusion of a monomer in a polymer ($\alpha = 1/2$), our model (equation (3.9)) generalizes the dynamics to yield any subdiffusion exponent. By controlling the value of χ in (3.12), the relative relaxation times of the modes are changed to yield different anomalous exponents. At times of the order τ_0 (the time it takes for the monomer to move a distance of b), the diffusion is normal with the monomer diffusion coefficient D_0, while at times longer than τ_N (the time it take for a monomer to diffuse its own radius of gyration), the monomer diffuses with the diffusion coefficient of the center of mass $D_{\text{cm}} = D_0/N^{\chi/2}$. These limiting times are given by:

$$\tau_0 = b^2/2D_0 \tag{3.13a}$$

$$\tau_N = R_g^2/D_{\text{cm}} = b^2 N^{1+\chi/2}/D_0. \tag{3.13b}$$

In the intermediate time regime $\tau_0 \ll t \ll \tau_N$, the monomer performs anomalous diffusion according to equation (1.1). At intermediate times, the monomers does not yet feel the full extent of the polymer. Therefore, its behavior in this regime does not depend on N. Simple scaling arguments can show [11], that the mean square displacement of an anomalous walker is of the form

$$\left\langle \Delta R_n^2 \right\rangle \approx b^{2-2\alpha} \left(D_0 t\right)^{\alpha}, \tag{3.14}$$

If we consider this equation for the two limiting times τ_0 and τ_N, the anomalous exponent is found to be

$$\alpha = 2/\left(2+\chi\right). \tag{3.15}$$

In our work, we solve equation (3.9) numerically for various values of χ, with different sets of boundary conditions. We perform the simulations in one dimension but the results can easily be extended to higher dimensions. Our simulation method is the Smart Monte Carlo algorithm which is a modification of the MC method, specifically applicable to conducting dynamical simulations. We elaborate on this in appendix B.

Figure 3.1 illustrates the motion of the central monomer in a polymer of size $N = 257$. The location of monomer $c = 129$ with respect to the starting location was squared and averaged over 10,000 independent simulations. The horizontal axis is in the characteristic time units τ_0, while the vertical axis is in units of b^2. These are the units we will work with

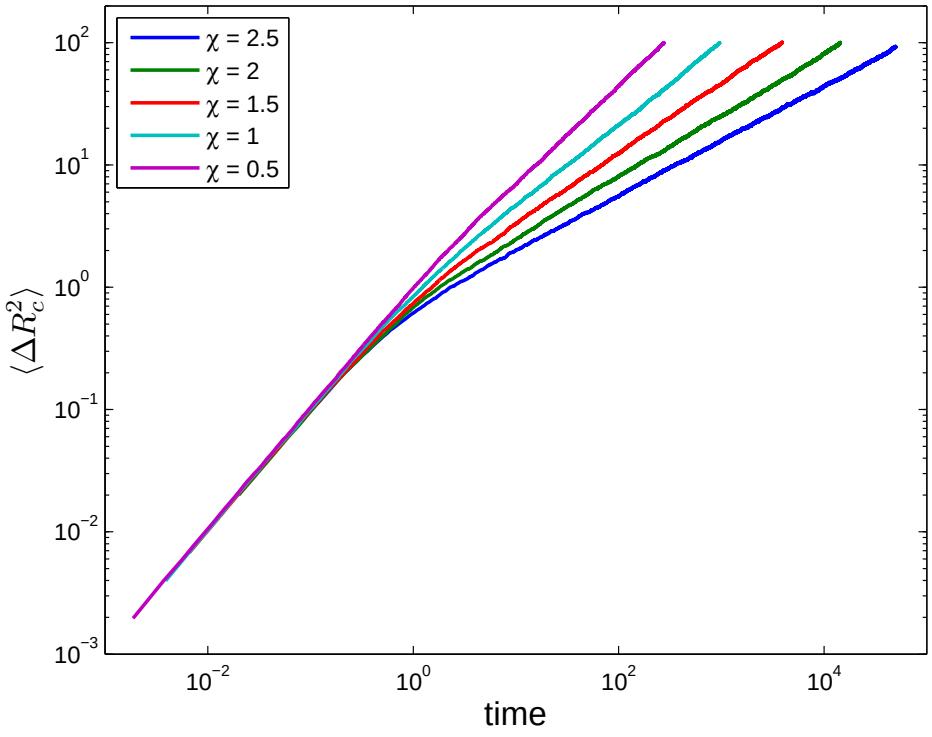

Figure 3.1: Variance of the central monomer $c = 129$ of $(N = 257)$ polymer. The curves match the values of: $\chi = 0.5, 1, 1.5, 2, 2.5$ going left to right. 10,000 runs where preformed for each exponent.

for the rest of this study. At times shorter than τ_0, the diffusion is normal and the curves for different values of χ coincide. The crossover from normal dynamics to anomalous is evident at about $t = \tau_0$ where the curves start to separate. As each of the lines is the simulation result for a different value of χ, we expect each curve to have a different slope. Indeed, the slopes of the lines behave according to expectations, giving smaller slopes for higher values of χ. Analyzing the slopes confirmed that they match the expectations (equation (3.15)). The crossover back to the linear regime does not appear in the figure because the system was not simulated for a long enough time.

Each of the modes behaves as an independent particle diffusing in a harmonic potential. The noise in the dynamical equation for each mode is defined through its mean and correlation, and can be described as a Gaussian. The probability distribution function (PDF) for each of the modes is also Gaussian. Since the position of the monomer R_n is a linear combination of Gaussian variables X_p (equation (2.20b)), it is clear that

its motion can also be described by a Gaussian process (this property of Gaussian processes is known from the Cramér's theorem [31]). At very short times, the variance of the monomer's PDF will be linear with time, as the mean square displacement is linear. In the anomalous regime, we know that the variance of the PDF has an anomalous dependence on time $\sigma^2 \propto t^\alpha$ ($\sigma^2 = \langle \Delta R_n^2 \rangle$). The PDF can be described by a Gaussian of the form

$$P(x,t) \propto e^{-\frac{(x-x_0)^2}{\text{const } b^{2-2\alpha}(D_0 t)^\alpha}}, \tag{3.16}$$

where x_0 is the initial position of the monomer. The variance in the anomalous regime can also be calculated analytically through a sum of the variances of modes [32]. At times larger than the τ_N, the variance also depends linearly on time, but with D_{cm}.

Anomalous processes have many unique features. The behavior when adding different boundaries condition differs dramatically from that of a single particle. Studying our model in the presence of one and two absorbing boundaries, we analyze the spatial probability density function and the absorption time probability density, and compare them to the results of other models.

Chapter 4

Tagged monomer dynamics in the presence of absorbing boundaries

4.1 Absorption time in the presence of two boundaries

First passage time (FPT) problems arise in many areas of physics where stochastic behavior is observed. In its simplest form it describes a Brownian particle that diffuses until it reaches a certain reactive site and a reaction takes place. More complex situations involve many reaction sites and interaction between particles. Typical examples of FPT processes are fluorescence quenching and neuron firing, or the purchase and sale of stocks when their value reaches a certain price [33]. The common property to all these processes is their termination when a certain value is reached. For many problems, the first passage phenomenon is modeled by the first passage probability $Q(t)$. This is the probability that a process was terminated at time t. In the case of a random walker, this is the probability that the walker hits a boundary for the first time at t. When the particle reaches the boundary, it disappears and the process stops. In terms of boundary condition, stopping the process when a certain point is reached is equivalent to placing an absorbing boundary condition at that point. First passage time and absorption processes are in fact, mathematically identical. We can also define the probability that a diffusing particle has

not yet hit the absorbing boundary at time t as its survival probability $S(t)$. The connection between the two quantities is given by

$$S(t) = 1 - \int_0^t Q(t')\, dt'. \tag{4.1}$$

The problem of a single diffusing particle in the presence of one or two absorbing boundaries can be solved analytically. Their solution are discussed in details by Chandrasekhar [34] and in [33]. I will review them here briefly.

Consider a particle starting from position $x_0 = 0$ at time zero. The diffusion equation for the probability density is

$$\frac{\partial P(x,t)}{\partial t} = D\frac{\partial^2 P(x,t)}{\partial x^2}. \tag{4.2}$$

For absorbing boundaries located at $X_{b1} = -L/2$ and $X_{b2} = L/2$, the solution is subjected to boundary conditions $P(-L/2,t) = P(L/2,t) = 0$. The solution of equation (4.2) may be written as the eigenfunction expansion of the operator at the right side of the equation, and a time dependent part

$$P(x,t) = \sum_{n=0}^{\infty} A_n \cos\left(\frac{(2n+1)\pi x}{L}\right) e^{-\left(\frac{(2n+1)\pi}{L}\right)^2 Dt}, \tag{4.3}$$

where A_n are determined by the initial conditions. Each of the eigenfunctions decays exponentially with a different relaxation time given by $\tau_n = \frac{L^2}{(2n+1)^2\pi^2 D}$. At long times, only the slowest eigenfunction survives and $P(x,t) = A_1 \cos\left(\frac{\pi x}{L}\right) e^{-\left(\frac{\pi}{L}\right)^2 Dt}$. The relaxation time $\tau_1 = L^2/\pi^2 D$ of the slowest mode is of the order of the characteristic time for diffusing the length of the interval between the walls. As a result, the asymptotic survival probability decays as

$$S(t) \propto e^{-\left(\frac{\pi}{L}\right)^2 Dt} \equiv e^{-t/\tau_1}. \tag{4.4}$$

The first passage time distribution can be characterized by its moments and the mean time to hit or exit the boundaries. The n-th moment of the distribution is given by

$$\langle t^n \rangle = \int_0^\infty t^n Q(t)\, dt. \tag{4.5}$$

The characteristic time scale for the first passage problems is L^2/D. For example, in the problem of a diffusing particle between two walls, the mean passage time is just $\tau =$

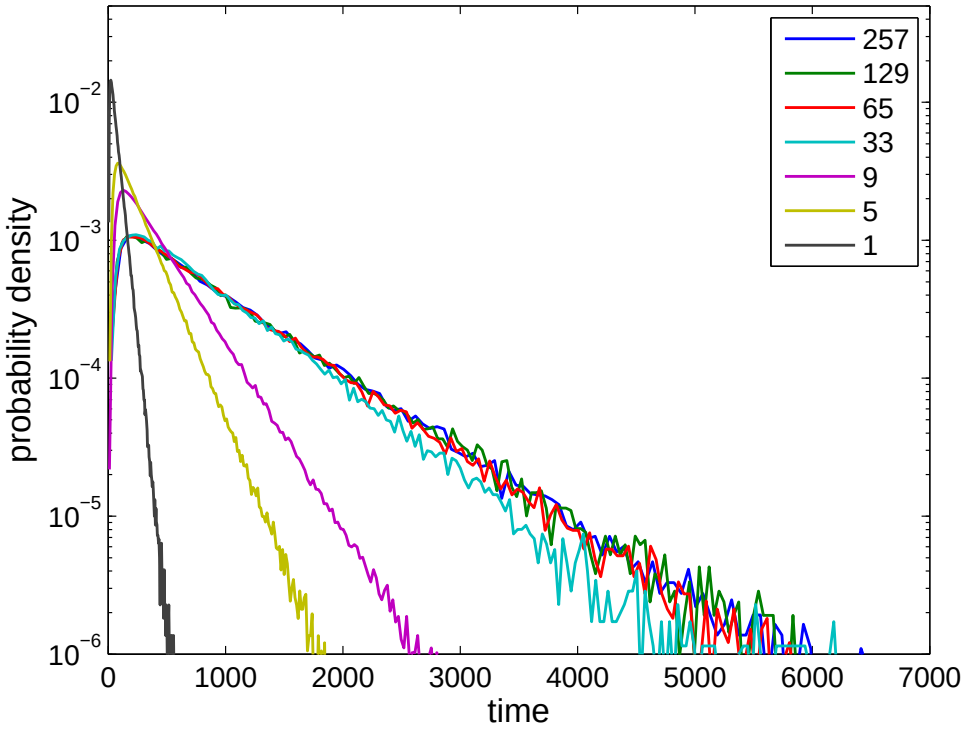

Figure 4.1: Probability distribution of the absorption time of the central monomer of Gaussian ($\chi = 2$) polymers of lengths $N = 1, 5, 9, 33, 65, 129, 257$ (plotted left to right). Two absorbing boundaries are present at $X_{b1} = -8$ and $X_{b2} = 8$. For each polymer length, 100,000 independent runs were preformed.

$L^2/8D$. When the particle starts its motion near the center of the interval, the moments of the first passage time behave as $\langle t^k \rangle \propto (L^2/D)^k$.

First passage time problems with anomalous diffusion have been studied extensively. Most models use Lévy type diffusion or the FDE to study the FPT distributions.

The dynamics of a tagged monomer in a polymer can be treated analytically, as we have shown in the previous chapters. However, the treatment cannot be extended to include absorbing boundaries. Although the equation for the monomer motion can be separated to independent Langevin equations for the modes, the introduction of boundaries in the real space couples the equations again. We use numerical methods to study the behavior of our model system in the presence of boundaries.

Let us introduce absorbing boundaries into our model system. We simulated the dynamics of Gaussian polymers ($\chi = 2$) of different lengths ($N = 2^l + 1$ where l is a natural

number) by solving equation (3.9) numerically using the SMC method. At every time step, we followed the motion of the central monomer ($c = 2^{l-1} + 1$) by transforming the modes amplitudes to the real space (equation (2.20b)) and checking if it had crossed the boundaries, i.e. has been absorbed. At $t = 0$, we located c at the origin while the entire polymer was at equilibrium and placed absorbing boundaries at $X_{b1} = -8$ and $X_{b2} = 8$. Figure 4.1 depicts the probability distribution of the absorption time (denote $Q(t)$) on a semi-log scale. We can see that for small polymers, the distribution is similar to that of a single particle with a diffusion constant of $D_{\text{cm}} = D_0/N$. This happens because, for small polymers, the radius of gyration is smaller than the length of the interval and the slowest relaxation time is smaller than the time it takes to diffuse the interval with the D_{cm}. The probability distribution of the absorption time for a single particle can be derived from equation (4.3) with the matching initial conditions. From the equation, it is clear that, for long times, the probability function decays exponentially with a time constant of $\tau \approx X_b^2/2D_{\text{cm}}$.

As we take longer polymers, the distributions start to coincide, until they overlap for polymers of lengths $N = 65, 129, 257$. This occurs because, for large polymers, the radius of gyration is larger than the boundary size and the longest relaxation mode exceeds the mean absorption time. For $N = 257$ for example, the slowest relaxation time is $\tau_1 \approx 1.3 \times 10^4$, while the characteristic time to diffuse the interval with anomalous exponent $\alpha = 1/2$ is $X_b^4/b^2 D_0 \approx 4 \times 10^3$. Because in this regime the distribution function becomes independent of the polymer size, we are guaranteed that the monomer's motion will be anomalous even at long times. This can also be observed in figure 3.1, where the diffusion is anomalous throughout the entire process.

Note that the asymptotic behavior of the absorption time distribution in figure 4.1 is clearly an exponential decay. This excludes the possibility of describing the distribution as a stretched exponential $\ln(Q(t)) \approx -t^{1/2}(D/X_b^2)^{1/2}$ at large times, as was previously proposed by Nechaev *et al.* [35].

Now let us see how the shape of the absorption time distribution function changes as we change the anomalous exponent. To do so, we simulated equation (3.9) with different values of χ, each produces a different exponent according to equation (3.15). Again, at the beginning of each simulation, monomer number 129 of an equilibrated polymer ($N = 257$) was placed at the origin and its location was followed in time. In figure 4.2, we

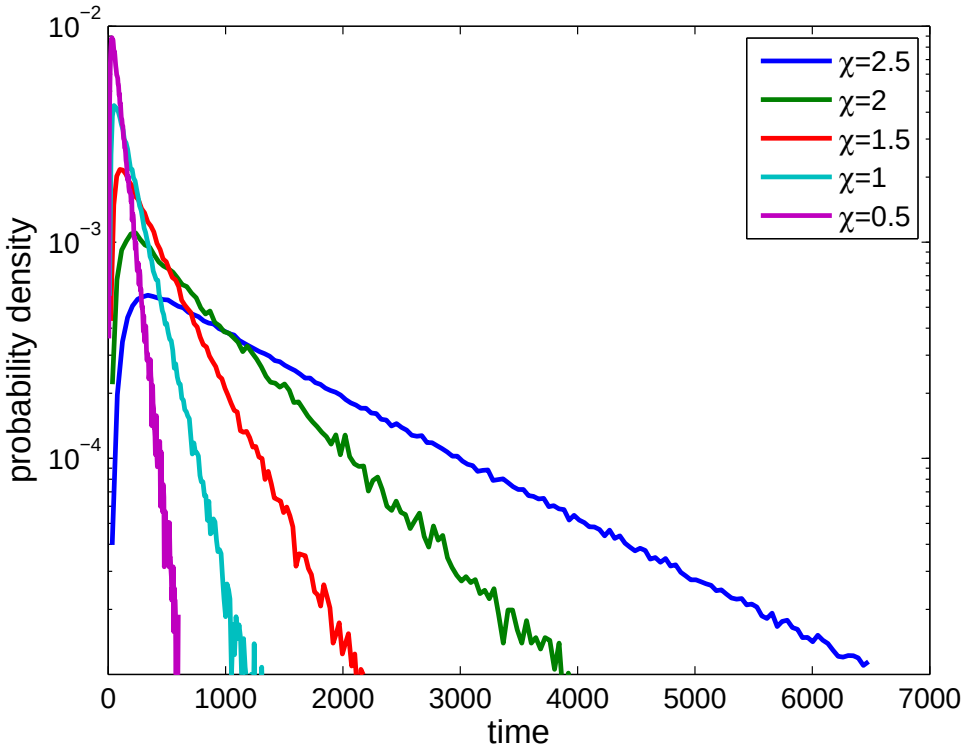

Figure 4.2: Probability density for the absorption times of a central monomer in a $N = 257$ polymer, in the presence of two absorbing boundaries set at $X_{b1} = -8$ and $X_{b2} = 8$. Each of the curves is the result of 100,000 independent simulation with a certain χ. The different curves correspond (from left to right) to $\chi = 0.5, 1, 1.5, 2, 2.5$.

illustrate in a semi-log plot, the results of the absorption time distributions. The distributions have the same general shapes. Since at large times the curves appear to be straight lines, it is evident that they still decay exponentially. However, the time scale, differs for each of the curves. Because of the exponential decay, its time constant should be of the same order as the mean absorption time. In the N-independent regime, we would expect the constant to depend solely on the exponent and on the time scale of the problem.

Previously, it was shown by Yuste *et al.* [36] and Gitterman [37] that, for subdiffusion processes described by the fractional diffusion equation, the absorption time distribution decays in large times as a power law and that the mean time of absorption is infinite. In our subdiffusion process, this is not the case. As the distribution decays exponentially for large time, we are guaranteed that the distribution has a converging first moment. Because we are in the infinite N regime (the distribution shape has no N dependence), the mean time can depend only on the length of the interval (the distance from the boundaries to the initial point), the monomer's diffusion coefficient, and the anomalous exponent. From the equation for the mean square displacement (3.14), we expect it to be of the order

$$T \approx D_0^{-1} \left(L/b^{1-\alpha} \right)^{2/\alpha} . \tag{4.6}$$

In fact, since this is the only time scale in our problem, we expect all our characteristic times to be of the same order. In figure 4.3 are depict three characteristic times of our system: the exponential decay constant of the absorption time distribution, the calculated first moment of the distribution and the theoretical time constant T as calculated from equation (4.6) with $L = 8b$ and $D_0 = b^2/\tau_0$. We plotted these times as a function of the anomalous exponent. The decay constant and the mean absorption time give very similar results. The difference between them results probably from the way we chose the data points for analysis. Comparing them to T, we see that the curves behave differently for smaller values of α, whereas for higher values the curves have similar slopes. It seems that as α goes to 1, the curves are similar up to a constant that does not depend on the exponent. In the same way that the characteristic time in the single particle problem differs from the mean absorption time in a prefactor, we expected to see a difference in our case. In principle, it is possible that the prefactor would have a certain dependence on α. This behavior creates the different slopes for the curves.

Contrary to the result of the fractional diffusion equation, we get a finite mean absorption time in our subdiffusion process. This implies that if it would have been possible to describe our model by an operator equation in the real space, it would not be the fractional diffusion equation.

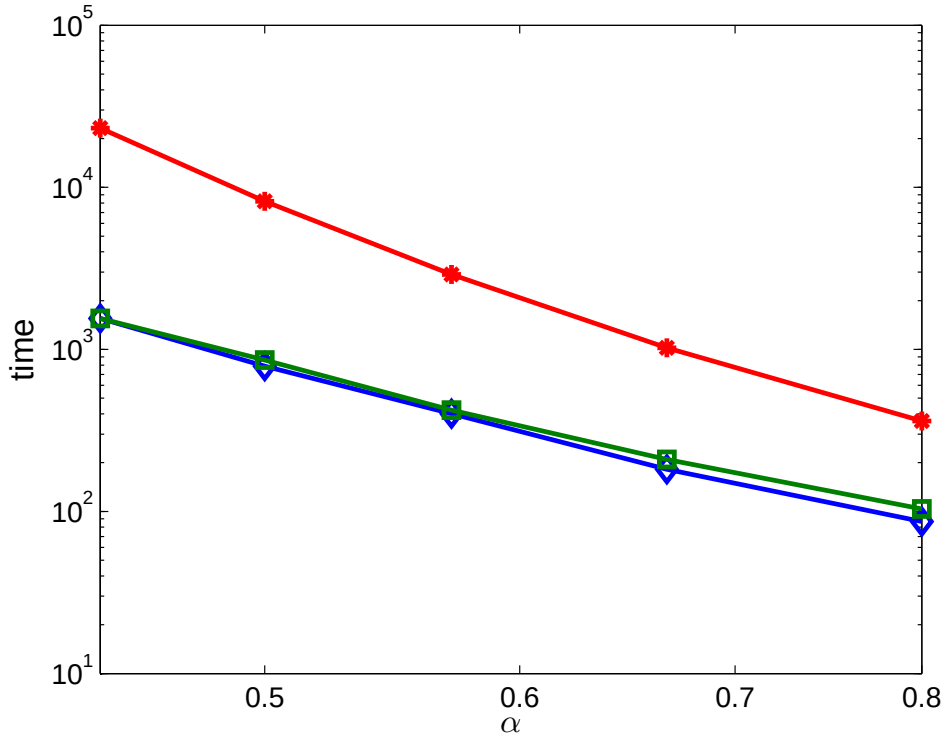

Figure 4.3: Comparison between the mean absorption time (squares) with the exponential decay time constant (diamonds) as calculated from the data shown in figure 4.2. Also shown is T (asterisks) as calculated from equation (4.6) with $L = 8b$ and $D_0 = b^2/\tau_0$

4.2 Absorption time in the presence of one boundary

Now we turn our attention to the behavior of our model in the presence of a single absorbing boundary. We begin by reviewing the problem of a single particle performing normal diffusion in the presence of one absorbing boundary. A detailed description can be found in Chandrasekhar's article [34].

Consider a particle performing normal one-dimensional diffusion starting from location $x_0 > 0$. An absorbing boundary located at the origin $X_b = 0$, sets the probability distribution function of the particle to be zero at that location. The most convenient way to solve the differential equation with this boundary condition is using the images method. We can place an image particle with a negative probability distribution function at the location $x = -x_0$ at the beginning of the process. We allowed both particles to diffuse freely in the whole space. The addition of the image fulfills the boundary condition for which $P(x = 0, t) = 0$. The probability distribution for the two particles can be written as the sum of Gaussians of two freely diffusing particles located respectively at x_0 and $-x_0$ where the PDF of the image particle has a negative sign

$$P(x,t) = \frac{1}{\sqrt{4\pi Dt}} \left[e^{-(x-x_0)^2/4Dt} - e^{-(x+x_0)^2/4Dt} \right]. \tag{4.7}$$

The absorption time distribution is given by the flux at the boundary. It can be derived from the probability distribution (4.7)

$$Q(t) = -D \frac{\partial P(x,t)}{\partial x}|_{x=0} = \frac{x_0}{\sqrt{4\pi Dt^3}} e^{-x_0^2/4Dt}. \tag{4.8}$$

In the long time limit $\sqrt{Dt} \gg x_0$, when the diffusion length is much bigger than the initial distance to the boundary, the absorption time distribution behaves as a power law $Q(t) \propto t^{-3/2}$. Because the first moment of the distribution diverges, the mean time to reach the boundary is infinite. The first moment diverges because the distribution has a long tail, a similar behavior to that of CTRW, where the waiting time distribution decays as a power law.

We return now to our model. We wanted to investigate the diffusion of the tagged monomer in the presence of a single absorbing boundary for different anomalous exponents. We performed simulations in which a single absorbing boundary was placed at $X_b = -8$ and the central monomer $c = 129$ of a polymer $N = 257$ was placed at the origin

$x_0 = 0$ at $t = 0$. As we have already shown for the case of two boundaries, we are in the infinite N regime, where the radius of gyration of the polymer is of the order of the distance to the boundary (the same numeric estimations apply). In this regime, the polymer is sure to perform anomalous diffusion throughout the process. We also performed simulation for polymers of different lengths and saw the congruence of the absorption time distributions for large polymers (data not shown). At very long times, unabsorbed monomers will probably diffuse far away from the boundary, and their diffusion at this regime would be normal. That happens when the time is considerably large than τ_N, and in our simulations we do not reach this time limit.

Figure 4.4 depicts the absorption time probability distributions of the tagged monomer for different values of χ in a logarithmic plot. Also shown is the absorption time distribution of a single particle performing normal diffusion (equation (4.8)). For small values of χ, the exponent approaches the normal diffusion limit, and we see that the probability density resembles that of a single particle. At large times, the probability density clearly behaves as a power law. This result can be compared to the study of Ding *et al.* [38], which investigated a CTRW using the fractional Fokker-Planck equation in subdiffusion and superdiffusion. In their study, one absorbing boundary is placed at the origin and the other at infinity which makes it a one absorbing boundary problem. Ding *et al.* derived an expression for the absorption time distribution and give an expression for its asymptotic behavior at large times:

$$Q(t) \propto t^{-1-\alpha/2}, \tag{4.9}$$

where α is the anomalous exponent. In the case of normal diffusion where $\alpha = 1$, we get the expected power law behavior of $-3/2$ of equation (4.8).

In figure 4.4, we drew over the distributions, lines with the expected power law as specified by equation (4.9). The fit between the curves and the long time behavior is very good. While the absorption time probability density with two boundaries decayed exponentially in the long time limit, which was in disagreement with the results of FDE, here we see that the long time behavior matches that of FDE.

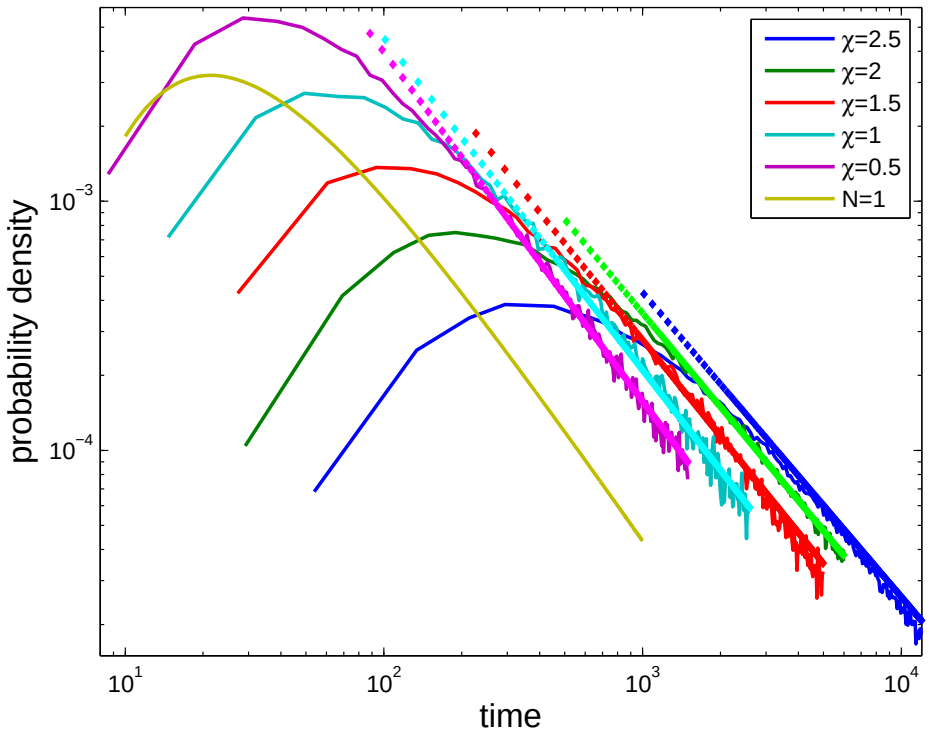

Figure 4.4: Absorption time distribution of monomer $c = 129$ of a polymer $N = 257$, in the presence of an absorbing boundary at $X_b = -8$. The curves correspond to $\chi = 0.5, 1, 1.5, 2, 2.5$ going left to right. For each χ value, 100,000 independent runs were performed. The leftmost curve corresponds to the absorption distribution of a single particle performing normal diffusion under the same initial and boundary conditions. The dotted lines give the large time approximation of the distribution corresponding to equation (4.9).

4.3 Probability density in the presence of one absorbing boundary

In the following chapters, we consider the probability distribution function (PDF) of the tagged monomer position in the presence of absorbing boundaries. We begin with the case of a single boundary.

In the previous chapter we showed that the problem of a single particle performing normal diffusion under the influence of one absorbing boundary can be solved using the addition of an image particle. When we have a particle performing Lévy flights (which would result in anomalous diffusion), the use of this method is more problematic. The method of images is expected to work only when the boundary is also a turning point of the trajectory, i.e. when the particle cannot pass the boundary without being absorbed. In the case of LF, the particle can perform a long jump that would take it far across the boundary. That is the reason the image method fails in this case [32, 39].

Our model is a non-Markovian process. At every time step, the monomer's position is the Fourier transform of the Rouse modes amplitudes. Since each of the modes changes on a different time scale, sequential steps depend on one another. The application of the image method assumes that steps are independent. Thus it does not work for our subdiffusion system.

Figure 4.5 depicts the probability distribution function for the central monomer of a Gaussian polymer ($\chi = 2$) of length $N = 257$ with an absorbing boundary present at $X_b = -8$. As the times in which we simulate are short then τ_N, we are guaranteed anomalous dynamics throughout the process. At the beginning of the simulation, the tagged monomer was placed at the origin and the polymer was equilibrated. The shape of the PDF is quite different from that of a single particle (equation (4.7)) performing normal diffusion. The PDF of a single particle is linear near the boundary, while the distribution in the figure is clearly not so. Thus, it is evident that the use of the image method is not applicable here.

At long times, the distribution exhibits self-similarity. We can show that by rescaling the distributions from figure 4.5. Let us introduce a new variable $\rho = (x - X_b)/t^{1/(2+\chi)}$, where x is the position of the tagged monomer and t is the time. The result of the scaling after normalization is illustrated in figure 4.6. We can understand this behavior if

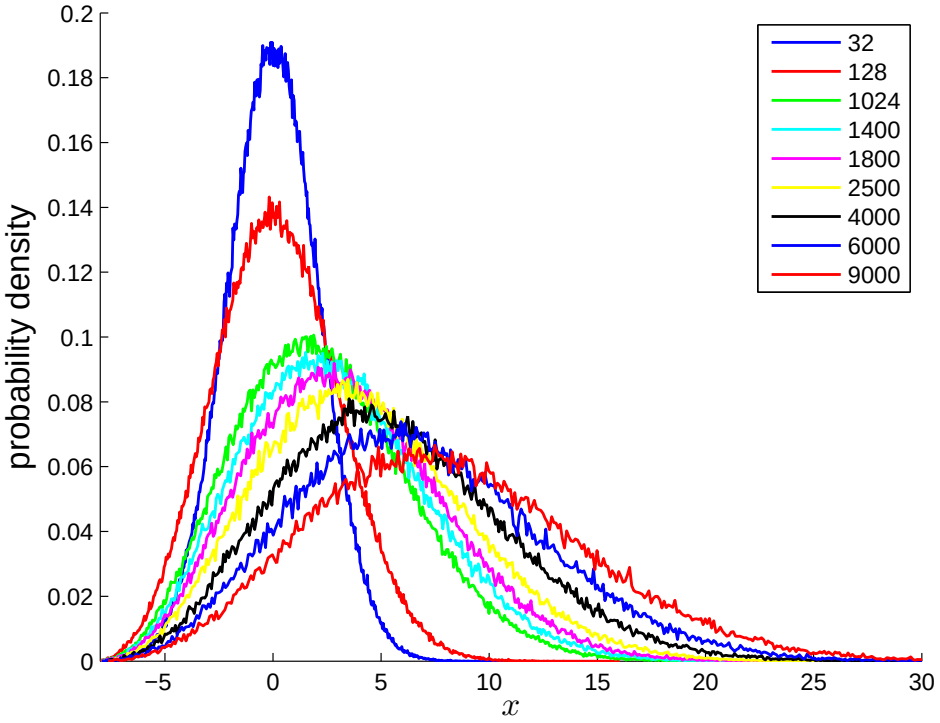

Figure 4.5: Probability density function of the central monomer in a polymer $N = 257$. An absorbing boundary was located at $X_b = -8$. The curves correspond (narrow to broad) to different times, as shown in the legend. The distribution was obtained by 100,000 independent runs.

we recall the dependence of the mean square deviation on time (equation (3.14)) in the absence of absorption and observe the shape of the PDF in the anomalous regime (equation (3.16)). Since the size $\sqrt{\langle R^2(t)\rangle}/t^{1/(2+\chi)}$ is constant, after the rescaling, the probability density losses at long times its time dependence.

The probability density of the tagged monomer might be described as the eigenfunction of some linear operator in the real space, with corresponding boundary condition (in our case one or two absorbing boundaries). However, our model is defined in the Fourier space while our boundary conditions are described in the real space. From our results so far, we know that this operator is not the FDE. We are not even sure if it is linear. We have, however, some intuition about its origin. In the section describing the physical motivation for our model (3.1.1), we showed that the Langevin equations of Rouse model, along with a distance-dependent interaction that couples the velocities of the monomers,

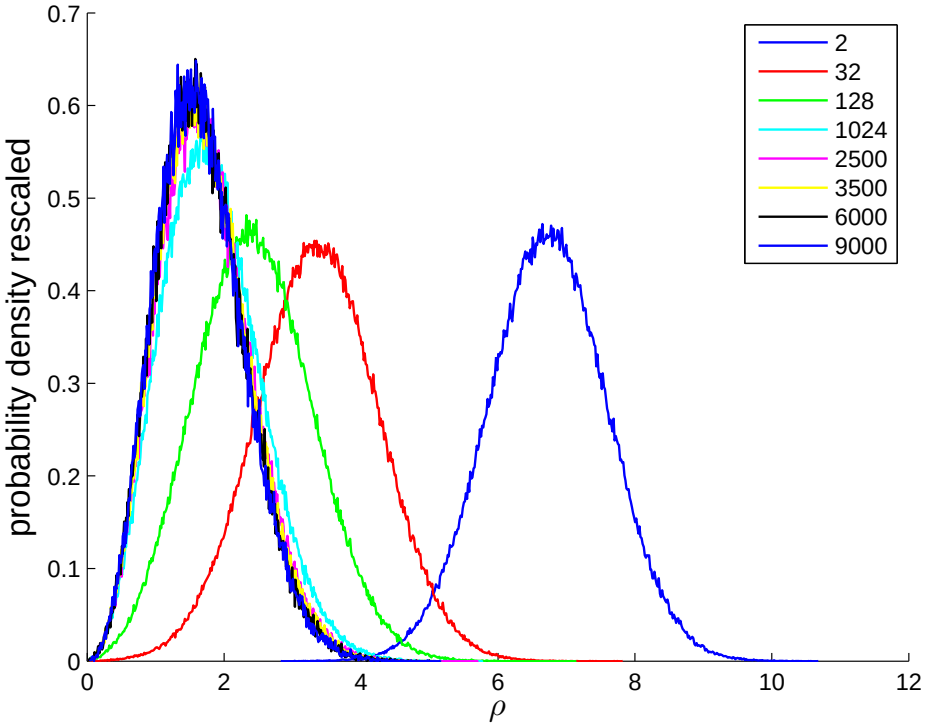

Figure 4.6: The probability density functions from figure 4.5 were scaled with the new variable $\rho = (x - X_b)/t^{1/(2+\chi)}$. The graphs coincide at long times.

can generate our dynamical equations in the continuous long chain limit.

Let us assume that there is a linear operator that describes our model. It can be solved as a form of an eigenvalue problem, with its solution given by:

$$P(x,t) = \sum_k A_k \psi_k(x)\, e^{\lambda_k t}, \tag{4.10}$$

where $P(x,t)$ is the probability density function, $\psi_k(x)$ are the eigenfunctions, λ_k are the eigenvalues and A_k are set by the initial conditions. As we do not even know the operator producing these solutions, it is impossible to derive an analytical expression for the eigenvalue problem. We investigated the properties of the solutions numerically. The natural time scales of our system are the relaxation times of the different modes. It is reasonable to assume that each of the eigenvalues corresponds up to some factor, to one of the Rouse mode relaxation times ($|\lambda_k| \approx 1/\tau_k$). At long times $t > \tau_1$ all the eigenfunctions have decayed exponentially, and we are left with the ground state eigenfunction ψ_1.

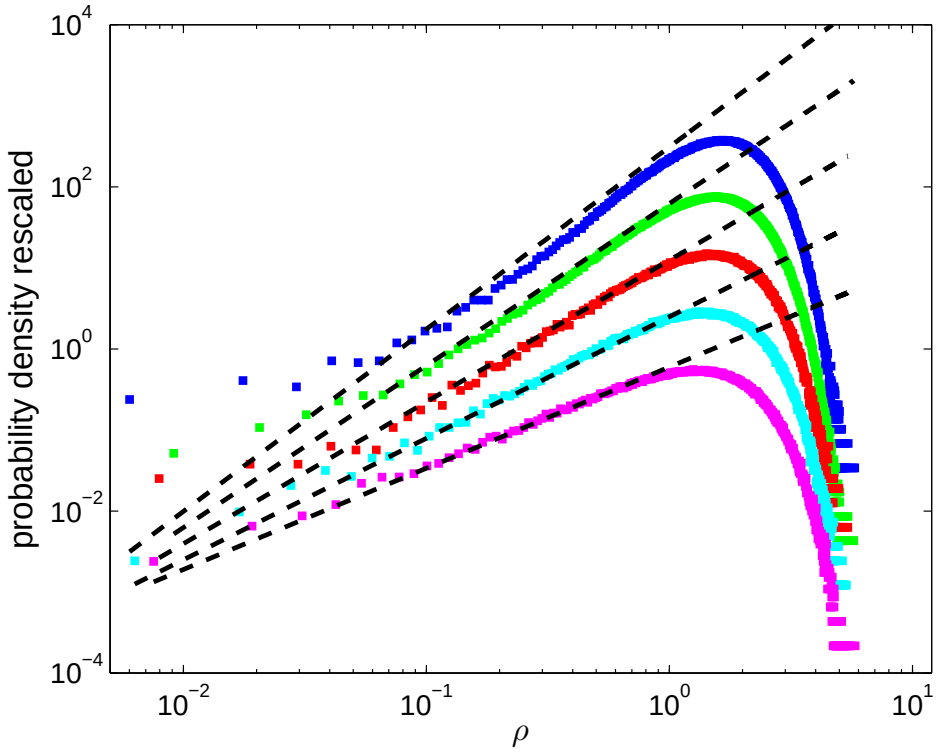

Figure 4.7: Probability density function of the central monomer $c = 129$ in a polymer with $N = 257$ monomers in the presence of one absorbing boundary. The horizontal axis is in the scaled variable ρ. The different curves correspond to $\chi = 0.5, 1, 1.5, 2.5$ (bottom up). The dotted lines give the small ρ approximation from of equation (4.11). The graphs are shifted vertically for clarity with increasing χ values by a factor of 5.

Figure 4.7 depicts the shape of the PDF of the central monomer ($N = 257$) in a logarithmic plot. To investigate the dependence of the PDF on the anomalous exponent, we ran simulations using different values of χ. The long time behavior of the PDF is shown, which matches to the ground state eigenfunction. After rescaling, the boundary is mapped to $\rho = 0$ and the density function does not change with time. Since, for longer times, in most of the realizations the central monomer has already been absorbed, it is difficult to gather enough data to produce a accurate curve which can be analyzed. To compensate for this, we used the fact that, after a certain time the shape of the distribution does not change. When calculating the PDF, we accumulated data from several large times. Although the samples at different times are somewhat correlated, the correlation seems to decay rapidly - enabling us to get better statistics.

Other works on anomalous diffusion in the presence of absorbing boundaries have calculated the PDF of their process [40]. The PDFs of Lévy flights and Lévy walks are usually sharply peaked, described by Fox functions [1] and look very different from the Gaussian probability distribution of the normal Brownian motion. In the study of Zumofen and Klafter of Lévy walks with a single absorbing boundary [41], the PDF near the boundary is shown both analytically and numerically to behave as a power law. Our results show that for small ρ, the PDF converges to the power law:

$$P(\rho) \propto \rho^{(2+\chi)/2} = \rho^{1/\alpha}. \tag{4.11}$$

This is the same scaling dependence on the anomalous exponent that Zumofen and Klafter found in their study. This also corresponds to the linear behavior of the PDF in the case of normal diffusion with one absorbing boundary (for $\alpha = 1$). The predicted scaling of ρ by equation (4.11) is shown in the figure as dashed lines. The simulation results indicate (figure 4.7) that the convergence towards the power law behavior near the boundary is slow for small ρ. Also, note that the convergence is faster for smaller values of χ. Very close to the boundary, the results should be handled with care. We performed our simulations with a finite time step, which in turn determines the mean size of the monomers' step. At distances from the boundary of the order of the step size, the discrete nature of the stepping mechanism emerges. For example, although we know that the PDF should be exactly zero at the boundary, we can see in the figure that this is not the case. For this reason, data points very close to the boundary should be ignored.

4.4 Probability density in the presence of two absorbing boundaries

Next we consider the behavior of the central monomer of a polymer between two absorbing boundaries. Figure 4.8 illustrates the probability distribution of the central monomer of a Gaussian polymer ($\chi = 2$) with $N = 257$ in the presence of two absorbing boundaries located at $X_{b1} = -8$ and $X_{b2} = 8$. In the figure, we see the evolution of the distribution in time. At very short times ($t \ll \tau_0$), the particle's distribution is Gaussian with the variance $\sigma^2 \propto t$. Later on, at times considerably shorter than the mean time of absorption,

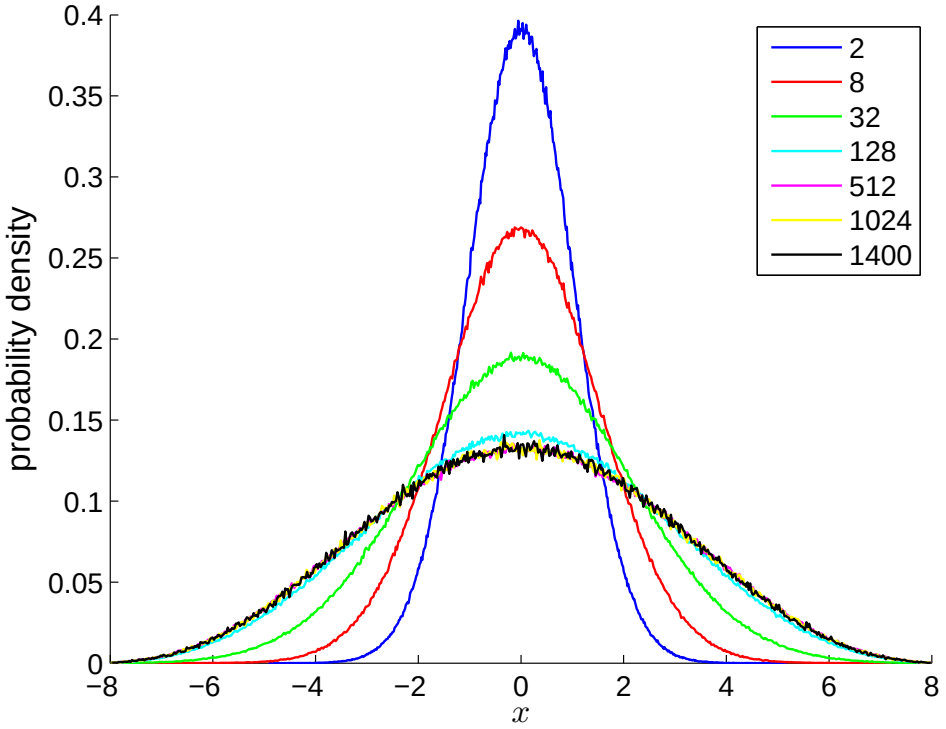

Figure 4.8: Probability density function of the central monomer in a Gaussian polymer with $N = 257$ monomers in the presence of two absorbing boundaries at $X_b = \pm 8$. The distribution is shown at different times $t = 2, 8, 32, 128, 512, 1024, 1400$ (narrow to broad). The distribution was obtained by 100,000 independent runs.

the particle is still unaware of the presence of the boundaries and performs anomalous diffusion with Gaussian distribution with $\sigma^2 \propto t^{1/2}$. Analogously to equation (4.10), it appears that at long times, only the slowest "eigenmode" survives and the shape of the normalized PDF stabilizes. In the long-time solution for normal diffusion (equation (4.3)), the slowest mode is a cosine with a period twice the length of the distance between the boundaries. This is clearly not the shape of the curve in the figure. It is also not a Gaussian (as the Gaussian value is never zero). Actually, we cannot describe the distribution with an analytical expression.

The method of images can be used to find the PDF of a normal diffuser between two absorbing boundaries using an infinite number of images farther and farther from the origin. The contributions of the additional images become progressively smaller and the PDF converge to a steady form. We cannot solve the non-Markovian motion of the tagged

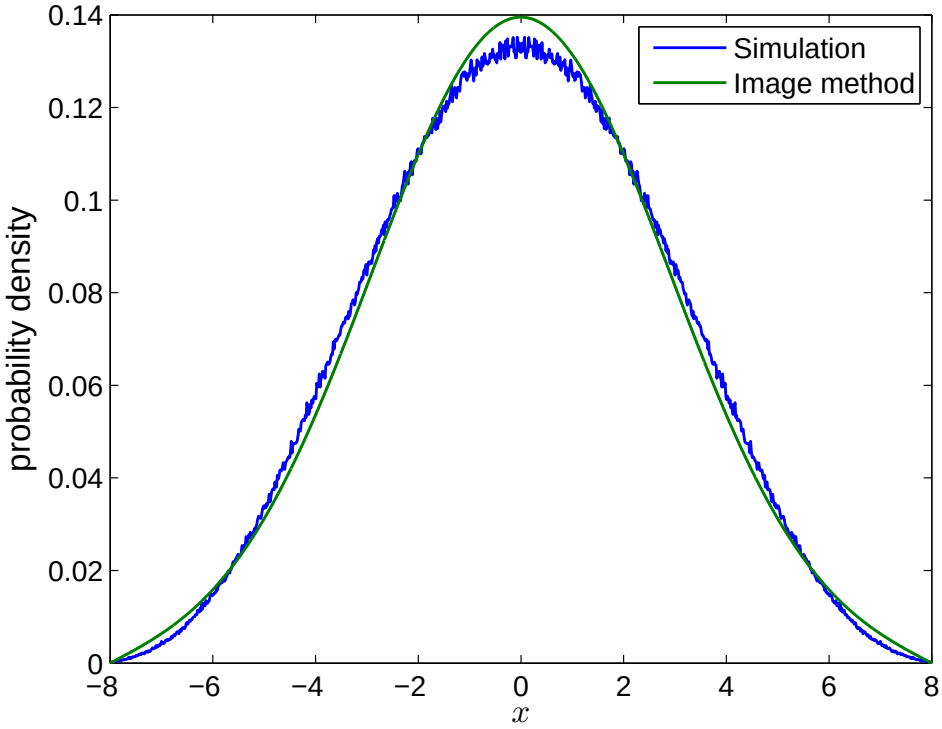

Figure 4.9: PDF for the central monomer in a $N = 257$ Gaussian polymer with absorbing boundaries (blue) compared with a PDF obtained by the image method with the same variance. Note that the graphs do not coincide.

monomer with this method. In figure 4.9 we present the long-time stable shape of the PDF from figure 4.8 and the PDF calculated by the method of images. To produce it, we placed particles at with a positive sign PDF at $x = 0, 32, -32$ and particles with negative sign PDF at $x = 16, -16$. The PDF of each particle was a Gaussian with the mean value set to be the position of the particle and variance of 1. We summed the Gaussian of all the particles. Since the PDF converges rapidly, no additional images were needed. To compare the two distributions, we changed the variance of the image distribution so that it would match that of the distribution obtained from the simulations and normalized it. We can see that the two curves do not match. The behavior of the image distribution is linear near the boundaries while the tagged monomer's distribution is not. This proves that, indeed, the method of images fails to solve our problem.

Next, we investigate the behavior of the probability density as χ is changed. Figure 4.10 depicts the shape of the "ground state eigenfunction" PDF of the central monomer

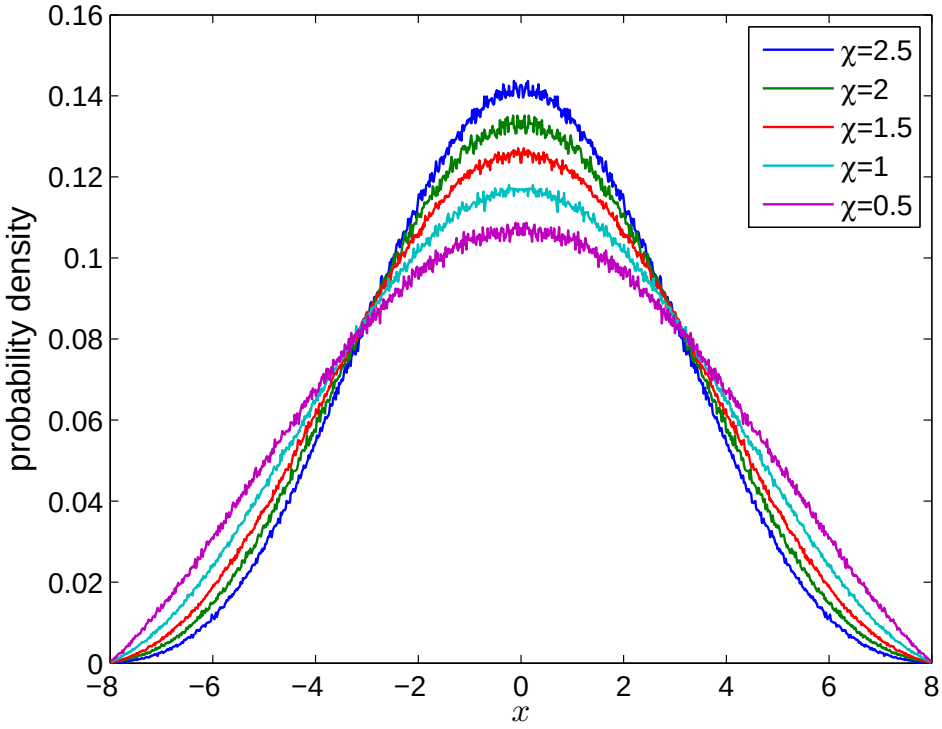

Figure 4.10: Probability density function of the central monomer in a polymer with $N = 257$ monomers with absorbing boundaries at $X_b = \pm 8$, for $\chi = 0.5, 1, 1.5, 2.5$ (bottom up). Each graph is the product of 100,000 independent runs.

in a polymer $N = 257$, for different values of χ. The limiting behavior of $\chi \to 0$ is that of a single particle - the PDF becomes the cosine function. In the other limit of $\chi \to \infty$ the distribution will give us a delta function.

Although we cannot get a closed analytical expression for the PDF, other studies that investigated the probability density function of anomalous processes showed that, near the boundaries, the PDF behaves like a power law. Zoia *et al.* [32], investigated the diffusion equation with a fractional Laplacian with two absorbing boundaries. The operator was implemented in such a way that its eigenfunction and eigenvalue could be calculated numerically. Specifically, the shape of the long time eigenmode was found. Analysis of the function's behavior near the boundaries demonstrated that it has a power law dependence in the anomalous exponent α

$$\psi_1 \approx (x - X_{b1})^{1/\alpha} . \tag{4.12}$$

Again, the power law behavior is the same as in the case of a single boundary condition (equation (4.11)). The Laplacian operator can be represented as a Toeplitz symmetrical matrix. It was shown analytically, based on Widom's study on the eigen-problem in Toeplitz matrix [42], that in the limit of $\alpha \to 0$, the first eigenfunction can be approximated near the boundaries as

$$\psi_1 \approx \frac{\Gamma\left(3/2+2/\alpha\right)}{\Gamma\left(1+2/\alpha\right)}\left(\left(\frac{x}{X_{b1}}\right)^2-1\right)^{1/\alpha}, \tag{4.13}$$

which is consistent with the numerical result in equation (4.12).

Figure 4.11 illustrates the distribution from figure 4.10 on a logarithmic plot with the horizontal axis shifted by $-X_{b1}$. The PDF near the boundary behaves as

$$P\left(x\right) \approx \left(x-X_{b1}\right)^{(2+\chi)/2}, \tag{4.14}$$

which displays the same power law behavior near the boundary as equation (4.12). Also shown are dashed lines fitted to each distribution, corresponding to $x^{(2+\chi)/2}$. Very near the boundary, the distributions deviate from the expected power law and converge to the small x approximation farther along the axis. Note that the convergence for the power law is faster to for smaller values of χ, while for $\chi = 2.5$ the convergence is rather poor.

In our simulations, we produced different probability distributions for different values of χ. We wanted to find out if a distribution for a specific χ can actually be calculated from the solution for another χ by some change of variables or a rescaling of some kind. Through algebraic analysis of the dynamical equations (3.9), one can see that it is not possible to define an effective time variable, such that χ will be scaled out of all the equations. By analyzing the distribution in figure 4.10, we can also show that the distribution for one χ cannot be calculated from that of another. Based on the small x approximation (equation (4.14)), we wanted to match the power law behavior of all the distribution to that of the distribution for the Gaussian polymer ($\chi = 2$). We raised all the other distributions to the power of $\frac{4}{(2+\chi)}$ and normalized them. The result is presented in figure 4.12. We see that the distribution are similar but they do not collapse. This indicates that the process is unique for every χ in the same way the eigenfunctions in the fractional Laplacian problem are unique for every α.

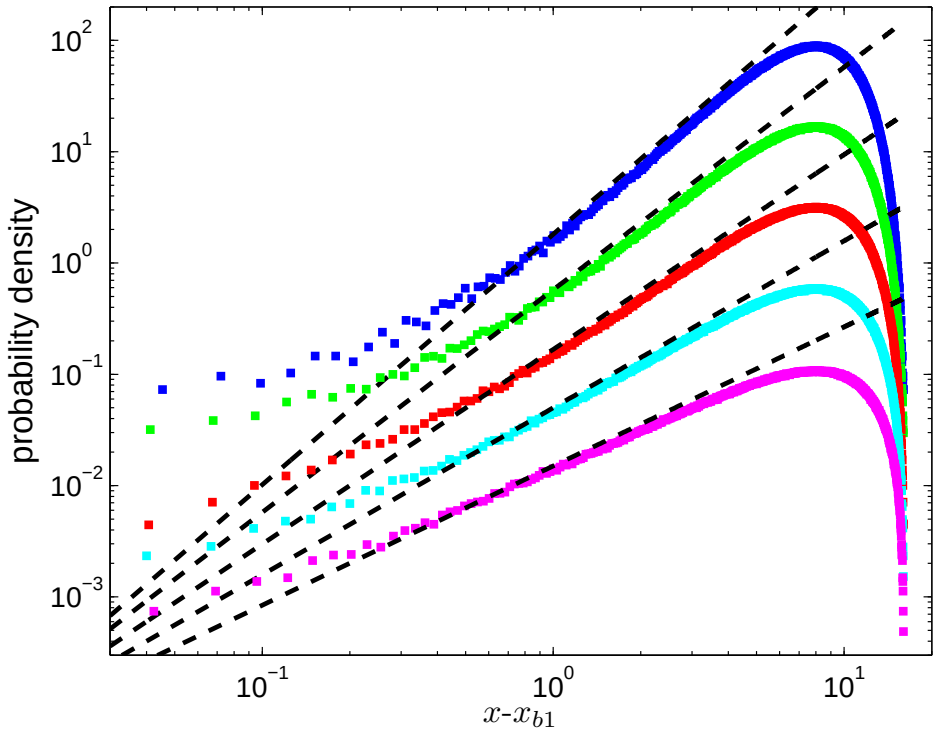

Figure 4.11: Probability density function of the central monomer in a polymer with $N = 257$ in the presence of absorbing boundaries at $X_{b1} = -8$ and $X_{b2} = 8$, for $\chi = 0.5, 1, 1.5, 2.5$ (bottom to top). The dashed lines give the small x approximation $x^{(2+\chi)/2}$. Each curve is the product of 100,000 independent runs. The curves are shifted vertically for clarity with increasing χ values by a factor of 5.

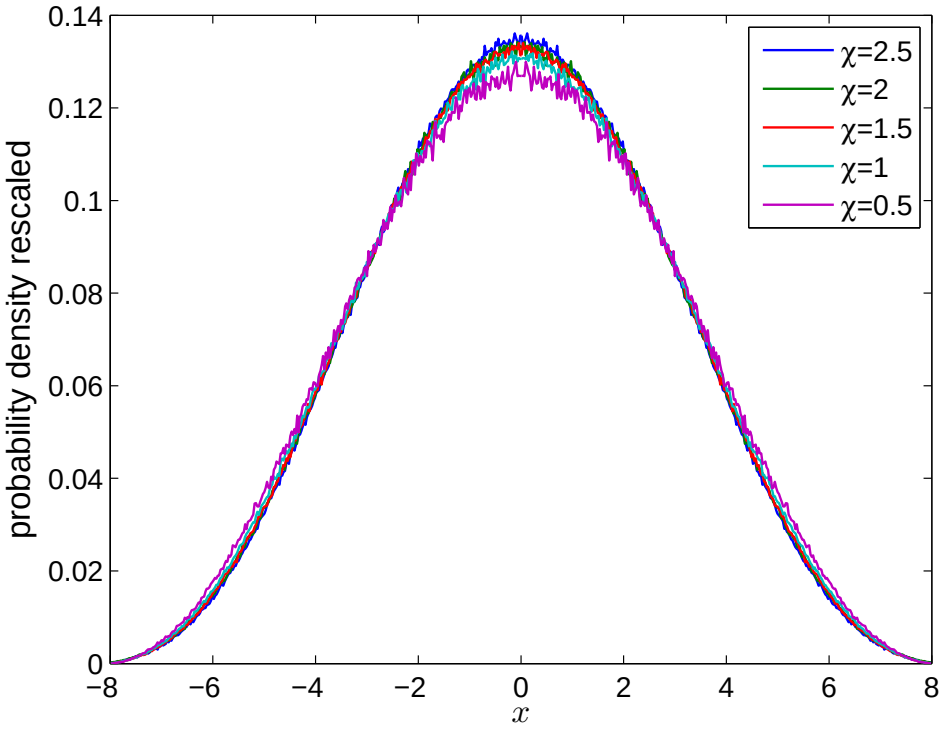

Figure 4.12: The probability densities from figure 4.10 were rescaled to match the PDF for $\chi = 2$ by raising each of them to the power of $\frac{4}{(2+\chi)}$ to match them in the small x approximation of equation (4.14). Note that the curves do not collapse, thus demonstrating that the solution for each χ is unique and can not be calculated from that of another.

Chapter 5

Translocation

In this chapter we will discuss the similarities between the system of a tagged monomer in the presence of two absorbing boundaries and translocation. We begin by reviewing the translocation process.

There are many biological systems in which a polymer diffuses or is pulled through a pore in the lipid membrane of the cell. This process is known as *translocation*. Phages, for example, invade bacteria by taking advantage of existing channels in bacterial membrane and translocate their DNA through it [43]. Inside the cell, peptides translocate into organelles by specific channels. Lately, translocation has drawn much attention as a potential method to sequence DNA (read its nucleotide sequence). Deamer *et al.* [44, 45] introduced an experimental method for rapid DNA sequencing. The DNA is threaded through a bacterial channel (alpha-hemolysin) and the nucleotide residing in the pore can be identified by measuring the ionic current through the channel. This new method, though promising, still lacks the proper resolution to sequence DNA correctly.

A number of theoretical and numerical works have shed light on the translocation process. A common approach is to describe the dynamics of the process through a single dynamical variable which is the number of the monomer currently inside the pore. This variable is known as the translocation coordinate (denoted $s\left(t\right)$). The translocation is completed when the translocation coordinate is 0 or $N+1$, i.e. when the polymer has left the pore. As the polymer is threaded through the pore, it faces an entropic barrier [46]. Since the number of possible configurations is least when the polymer is halfway through the pore, the polymer has to surmount the barrier in order to complete its translocation.

Early works modeled the translocation process as a form of Brownian dynamics [47]. The process was described by the diffusion equation with $s\left(t\right)$ as the dynamical variable. In this formalism, the process resembles the diffusion of a particle between two absorbing boundaries. This Brownian model constitutes the mean translocation time to scale with the polymer's length N as N^2. However, it was argued by Kantor *et al.* [9], that the translocation cannot be faster than the relaxation time that scales as N^{α}, where $\alpha = 1 + 2\nu$ is larger than two, for a self-avoiding polymer performing Rouse dynamics. The slowest relaxation time is of the order of the time it takes for a polymer to diffuse its own radius of gyration and it is not reasonable to assume that the constraint of a pore would accelerate the process rather then slowing it down. The relaxation time sets an lower bound on the mean translocation time. The result was also corroborated by Monte Carlo simulations. Recent simulations in 3D have argued that the translocation is even slower [48], but the validity of these results has yet to be proven [49].

It is not clear what kind of equation would best describe the translocation process. It was argued [50] that it can be described by a fractional diffusion equation. This would result in an infinite mean translocation time. However, experiments and numerical studies indicate that the mean translocation time is well defined. Since our model also gave finite mean time of absorption for the case of two absorbing boundaries, it is reasonable to compare it with the translocation process.

The translocation process and the dynamics of a tagged monomer between two absorbing boundaries have certain similarities. In both processes, we follow the dynamics of a single dynamical variable - the translocation coordinate $s\left(t\right)$ and the position of the tagged monomer $R_n\left(t\right)$. In both cases, the variable performs anomalous diffusion because of its interactions with the other monomers, and its dynamics is governed by Rouse relaxation. While the tagged monomer diffuses in the real space until it is absorbed by one of the boundaries, the translocation coordinate diffuses in the discrete monomer number (index) space $(1...N)$ until one of its edges has diffused out of the pore and the polymer has fully translocated.

We decided to study the analogies between the processes by comparing their probability distribution functions. Simple scaling considerations [9, 51] suggest that the mean square displacement of the reaction coordinate scales with time as $\left\langle \Delta\left(s\left(t\right)\right)^2 \right\rangle \propto t^{\alpha}$ with $\alpha = 2/\left(1 + 2\nu\right)$ which is 0.8 in 2D.

We compared the PDF of the translocation coordinate of a 2D self-avoiding polymer of size $N = 128$ (data from Chatelain *et al.* [52]) with the PDF of the tagged monomer location as obtained from our model with $\chi = 0.5$ for the central monomer of polymer $N = 257$ (figure 4.10). As the two processes have the same anomalous exponent $\alpha = 0.8$, they are comparable. The result is presented in figure 5.1. The two dynamical variables were rescaled to $x \in [0, 1]$ for the purpose of comparison. Both distributions were obtained after a long time (with respect to the mean passage time). At this point in time, only the "slowest eigenmode" survived. The translocation PDF was obtained by a Monte Carlo simulation on a 2D lattice. The absorption time distribution indicated an exponential decay as does our model. Since, at long times, most of the polymers have already translocated, the statistics for the results are not very good.

We can see that the curves are mostly congruent. The main difference between them occurs near the boundaries where the function is expected to go to zero as a power law with an exponent of 1.25 (equation (4.14)). However, the translocation PDF decreases faster, with a power of ≈ 1.44 [52]. The logarithmic plot, in figure 5.2 shows that, the PDF produced by our model converges to the expected exponent, while the translocation PDF does not.

The high resemblance between the functions is promising. It is clear that the processes share many features. The translocation problem is still under debate in the scientific community. More and more complex simulations are being performed to investigate the dependence of the mean translocation time on the polymer length and relaxation dynamics of the polymers. Yet, no single equation which could describe it sufficiently well was found. Models such as ours might hint on some of the features of a future solution.

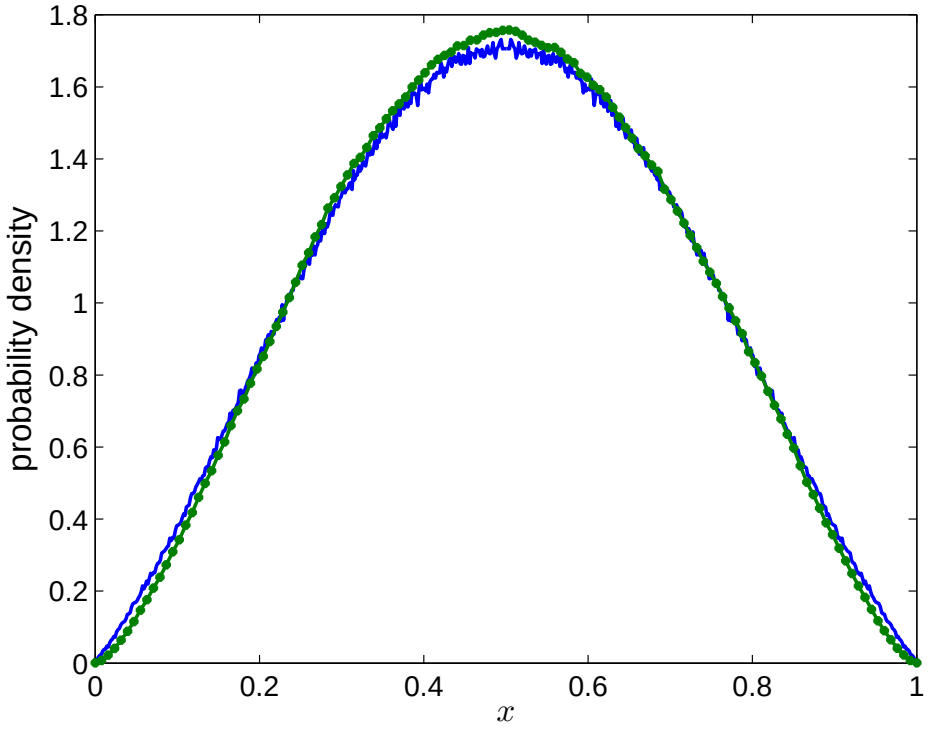

Figure 5.1: Probability density function of the central monomer in a polymer $N = 257$ monomers with $\chi = 0.5$ from figure 4.10 (ragged line). Probability density function of the translocation coordinate of a translocating polymer $N = 128$ (smooth line with circles). The data was taken from [52]). The two PDF's were shifted to $x \in [0, 1]$ to enable comparison.

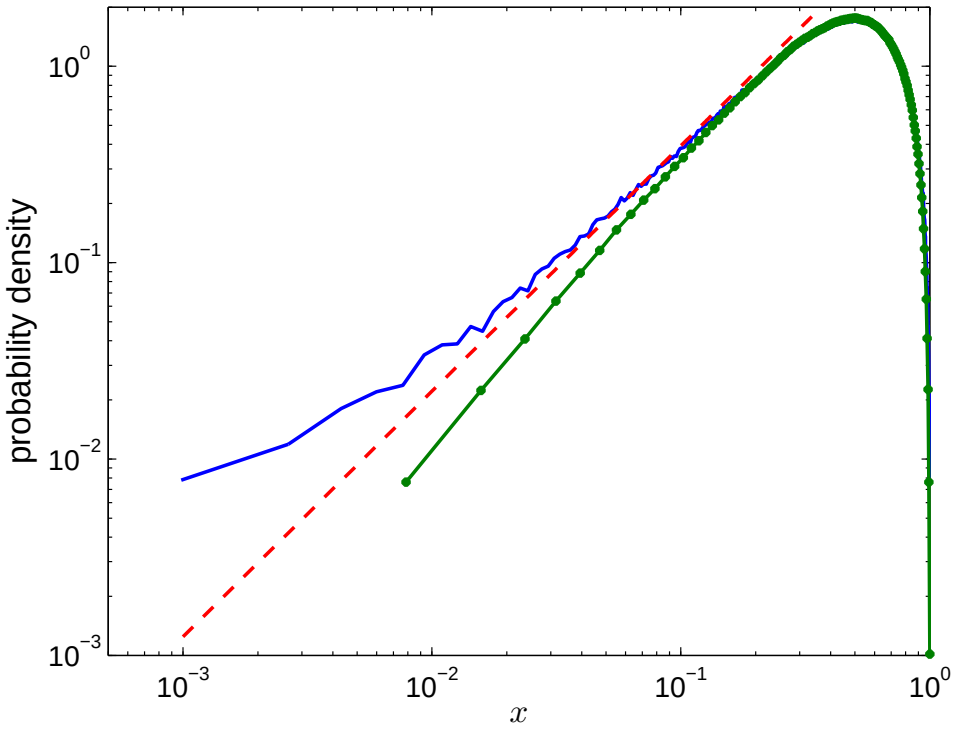

Figure 5.2: The same graphs as in figure 5.1 on logarithmic scale. The ragged line is the result of the our simulation with $\chi = 0.5$, while the smooth line with circles is the translocation PDF. Also shown (dashed line) is the power law behavior near the boundaries with exponent of 1.25.

Chapter 6

Conclusion

We have investigated the anomalous motion of a tagged monomer in a polymer. We examined the effect of a monomer-coupling interaction on the Rouse model. The interaction couples the motion of the monomers through their velocities, much like the hydrodynamical interaction, and its strength decays with distance between them as a power law with exponent χ. As it turned out, the addition of the interaction (under certain approximations) leads to the mean square displacement of the tagged monomer depending on time as $\langle \Delta R_n (t)^2 \rangle \propto t^\alpha$ with $\alpha = 2/(2+\chi)$. This motivated us to define a model in the Rouse (Fourier) space, that produces anomalous behavior of the tagged monomer with exponent α. The ability to control the exponent χ, enables us to get any subdiffusion exponent we desire. While most standard models used to investigate anomalous diffusion are motivated by mathematical concepts (fractional derivatives, for example), we developed a physical model which can be used to investigate subdiffusion processes. The dynamics of the monomers can be described in the Rouse space, where each mode changes on a different time scale depending on χ. From this dependence, the anomalous behavior emerges when transforming back to the monomer space.

Using simulation methods, we investigated the dynamics of the monomer in the presence of one and two absorbing boundaries, and found the absorption time distributions and the probability density functions. For one absorbing boundary, our model resembles the long-time behavior of absorption time distributions of other models. The power law tail in our model and its dependence on the anomalous exponent are similar to those found in other subdiffusion models (CTRW and fractional diffusion equation). For two

absorbing boundaries, our distribution decays exponentially in the long-time regime, and its decay time constant depends on the anomalous exponent. The time distribution has a finite mean, while, in fractional diffusion equation models and Lévy flights, the distribution has a power law tail and the mean time diverges.

We have also shown that the behavior of the PDF of the tagged monomer's position is similar to the known shape of PDF in other models. Near the boundaries, the PDF is expected to behave as a power law with an exponent of $1/\alpha$ (where α is the anomalous exponent). In our results, both for one and two boundaries, the PDF converges to the expected exponent, whereas the convergence is faster for smaller values of χ.

The translocation process shares many features with our model. We compared the PDF of the position of the tagged monomer with $\chi = 0.5$ to that of the translocation coordinate of a self avoiding polymer in 2D. The two curves are very similar in shape, but they differ in their behavior near the boundaries. In fact, the two processes are quite different in nature. Our polymer is equilibrated at all times, while the translocating polymer, in a way, is never at equilibrium. A process at equilibrium travels at all times through the same phase space. Yet, because the phase space in the translocation process is determined by the length of the strand on each side of the pore, the passage of a monomer changes it. It seems that our model cannot describe translocation precisely, as their probability distributions differ from one another. Nonetheless, perhaps it can suggest the structure of a future model that could give an exact description of translocation.

Appendix A

Treatment of polymer dynamics

A.1 The discrete cosine (Fourier) transform

Rouse equations can be decoupled by transforming them to the Fourier space. In our model, we work with a discrete polymer, composed of N monomers. In the Rouse model, the dynamics of each monomer is described by the Langevin equation. For the equations for the end monomers, $n = 1$ and N (2.17), to resemble those for the other monomers (2.16), we define additional hypothetical monomers

$$R_0 = R_1 \tag{A.1}$$

$$R_{N+1} = R_N. \tag{A.2}$$

We use the discrete cosine transform (DCT) [53] which fulfills the condition on the end monomers

$$X_p = \frac{1}{N}\sum_{n=1}^{N} R_n \cos\left(n-\frac{1}{2}\right)\frac{p\pi}{N}, \tag{A.3a}$$

$$R_n = X_0 + 2\sum_{p=1}^{N-1} X_p \cos\left(n-\frac{1}{2}\right)\frac{p\pi}{N}, \tag{A.3b}$$

where the set of mode functions are

$$\cos\left(n-\frac{1}{2}\right)\frac{p\pi}{N} \qquad n=1,...,N, \quad p=1,...,N-1. \tag{A.4}$$

We show that the functions form an orthogonal set. First let us find the following sum

$$S_n(\theta) \equiv \sum_{k=1}^{n+1} \cos\left(k-\frac{1}{2}\right)\theta. \tag{A.5}$$

We will solve it by using complex variable

$$e^{i\theta/2}\left(1+e^{i\theta}+...+e^{in\theta}\right)=\exp\left(i\frac{\theta\,(n+1)}{2}\right)\frac{\sin\left(\frac{\theta(n+1)}{2}\right)}{\sin\left(\frac{\theta}{2}\right)}.$$

After taking the real part of the above relation

$$S_n(\theta)=\frac{\sin(\theta(n+1))}{2\sin\left(\frac{\theta}{2}\right)}. \tag{A.6}$$

We note that

$$\begin{cases} S_n(\theta_p)=0 & \text{, for } \theta_p=\frac{p\pi}{n+1}\text{, and} \\ S_n(0)=n+1. \end{cases}$$

The inner product C_{lm} of two functions $\cos(l\theta_k)$ and $\cos(m\theta_k)$

$$C_{lm}=\sum_{k=1}^{n+1}\cos(l\theta_k)\cos(m\theta_k)=\frac{1}{2}\sum_{k=1}^{n+1}[\cos(l+m)\theta_k+\cos(l-m)\theta_k]=$$
$$\frac{1}{2}\left[S_n(\frac{(l+m)\pi}{n+1})+S_n(\frac{(l-m)\pi}{n+1})\right].$$

From this we get the functions orthogonality relation:

$$C_{lm}=\frac{1}{2}(n+1)\delta_{l,m} \tag{A.7a}$$

$$C_{00}=n+1 \tag{A.7b}$$

A.2 Langevin equation of Rouse modes

The one-dimensional over-damped Langevin equation for the location x of a particle, under the influence of an external potential U and a random force f is of the form

$$\frac{dx}{dt}=-\frac{\partial U}{\partial x}+f. \tag{A.8}$$

In the Rouse model, a polymer is described as a chain of monomers connected by harmonic springs. The Hamiltonian for N monomers is given by

$$H=\frac{\kappa}{2}\sum_{n=1}^{N-1}(R_n-R_{n+1})^2. \tag{A.9}$$

The Langevin equation for monomer n, influenced by the Hamiltonian is:

$$\zeta \frac{dR_n}{dt} = -\kappa(2R_n - R_{n+1} - R_{n-1}) + f_n \tag{A.10}$$

with the noise defined as:

$$\langle f_n(t) \rangle = 0 \tag{A.11a}$$

$$\langle f_n(t) f_m(t') \rangle = 2\zeta k_B T \delta_{n,m} \delta(t - t'). \tag{A.11b}$$

We use a white noise with zero mean and a correlation which depends on the friction constant. The Fourier and inverse Fourier transform of the random noise are respectively given by

$$f_p = \frac{1}{N} \sum_{n=1}^{N} f_n \cos(n - \frac{1}{2}) \frac{p\pi}{N} \tag{A.12a}$$

$$f_n = f_0 + 2 \sum_{p=1}^{N-1} f_p \cos(n - \frac{1}{2}) \frac{p\pi}{N}. \tag{A.12b}$$

Now we can present the Langevin equation (A.10) in Fourier space by inserting the Fourier transform of the variables:

$$\zeta \left[\frac{dX_0}{dt} + 2 \sum_{p=1}^{N-1} \frac{dX_p}{dt} \cos(n - \frac{1}{2}) \frac{p\pi}{N} \right] = -\kappa \left[4 \sum_{p=1}^{N-1} X_p \cos(n - \frac{1}{2}) \frac{p\pi}{N} - 2 \sum_{p=1}^{N-1} X_p \cos(n + \frac{1}{2}) \frac{p\pi}{N} \right.$$
$$\left. - 2 \sum_{p=1}^{N-1} X_p \cos(n - \frac{3}{2}) \frac{p\pi}{N} \right] + f_0 + 2 \sum_{p=1}^{N-1} f_p \cos(n - \frac{1}{2}) \frac{p\pi}{N}.$$

Because the mode functions are orthogonal, the equality in the above expression holds for every value of p. The equation for each mode (multiplied by N) is

$$2\zeta N \frac{dX_p}{dt} = -8N\kappa \sin^2 \left(\frac{p\pi}{2N} \right) X_p + 2N f_p, \tag{A.13}$$

The noise correlation in Fourier space is given by:

$$\langle f_p(t) f_{p'}(t') \rangle = \frac{1}{N^2} \sum_{mn} \cos(n - \frac{1}{2}) \frac{p\pi}{N} \cos(m - \frac{1}{2}) \frac{p'\pi}{N} \langle f_n(t) f_m(t') \rangle =$$
$$\frac{1}{N^2} \sum_{n} \cos(n - \frac{1}{2}) \frac{p\pi}{N} \cos(n - \frac{1}{2}) \frac{p'\pi}{N} 2\zeta k_B T.$$

By using (A.7) we get

$$\langle f_p(t) f_{p'}(t') \rangle = 2\zeta k_B T \delta_{p,p'} \delta(t-t') \frac{1}{2N}, \quad p = 1, 2, ..., N-1, \tag{A.14}$$

$$\langle f_0(t) f_0(t') \rangle = 2\zeta k_B T \delta(t-t') \frac{1}{N}. \tag{A.15}$$

If we define $W_p = 2N f_p$, equation (A.13) can be rewritten as

$$\zeta_p \frac{dX_p}{dt} = -\kappa_p X_p + W_p, \tag{A.16}$$

where $\zeta_p = 2\zeta N$, and $\zeta_0 = \zeta N$. The random variable W_p is now characterized by

$$\langle W_p(t) \rangle = 0, \tag{A.17a}$$

$$\langle W_p(t) W_{p'}(t') \rangle = 2k_B T \zeta_p \delta_{p,p'} \delta(t-t'). \tag{A.17b}$$

Equation (A.16) of each mode ($p \geq 1$) is the equation for a particle in an harmonic potential with noise. The modes relax with the characteristic time

$$\tau_q = \frac{\zeta_q}{\kappa_q} = \frac{\zeta}{12 k_B T} \left[\frac{b}{\sin^2(\frac{q}{2})} \right]^2. \tag{A.18}$$

The Hamiltonian for the model can also be written in terms of Rouse modes. In the Rouse space, the Hamiltonian is written as the sum of energies from $N-1$ independent harmonic springs, each with a different spring constant

$$H = \sum_{q=\frac{\pi}{N}}^{\frac{\pi(N-1)}{N}} \frac{1}{2} \kappa_q X_q^2. \tag{A.19}$$

A.3 Solution of Langevin equation in harmonic potential

Here we give some analytical results for Langevin equation of a particle in harmonic potential.

$$\frac{dx}{dt} = -\kappa x + f, \tag{A.20}$$

with the noise moments given in equation (A.11).

First we find the correlation between the value of $x\,(t)$ and its initial value $x(0)$:

$$\begin{aligned}
\langle x(t)x(0)\rangle &= \frac{1}{\zeta^2}\int_{-\infty}^{t} dt_1 \int_{-\infty}^{0} dt_2 \exp\left[-\frac{(t-t_1-t_2)}{\tau}\right]\langle f(t_1)f(t_2)\rangle \\
&= \frac{1}{\zeta}\int_{-\infty}^{t} dt_1 \int_{-\infty}^{0} dt_2 \exp\left[-\frac{(t-t_1-t_2)}{\tau}\right] 2k_BT\delta(t_1-t_2) \\
&= \frac{k_BT}{\kappa}\exp(-t/\tau)
\end{aligned}$$

Note that the equilibrium properties are independent on the friction constant ζ, and that the correlation decays exponentially with the characteristic relaxation time $\tau = \zeta/\kappa$.

The first moment and variance of the random variable x can also be calculated

$$x(t) = x(0)\exp(-t/\tau) + \frac{1}{\zeta}\int_0^t dt' \exp\left(-(t-t')/\tau\right) f\left(t'\right) \tag{A.21}$$

$$\langle x(t)\rangle = x(0)\exp(-t/\tau) \tag{A.22}$$

$$\begin{aligned}
\langle (x(t) - \langle x(t)\rangle)^2\rangle &= \frac{1}{\zeta^2}\int_0^t dt_1 \int_0^t dt_2 \exp\left(-(t-t_1+t-t_2)/\tau\right)\langle f(t_1)f(t_2)\rangle \\
&= \frac{1}{\zeta}\int_0^t dt_1 \exp\left[-2(t-t_1)/\tau\right] 2k_BT = \frac{k_BT}{\kappa}\left[1-\exp(-2t/\tau)\right]
\end{aligned} \tag{A.23}$$

Equation (A.23) describes the relaxation of the variance of a mode.

A.4 Approximate treatment of velocity-dependent interaction between monomers

In this section, we describe the physical motivation that led us to define our model. The Rouse model can be generalized by adding a long distance interaction. Since the monomers diffuse in a solvent, their movement results in a force on their nearby solvent known as the hydrodynamical interaction. The interaction couples the velocities of the

monomers. To include them into a the Rouse model, the monomer's Langevin equation is rewritten with a mobility tensor. The strength the hydrodynamical interaction decays with the monomer distance as $|\boldsymbol{R}_n - \boldsymbol{R}_m|^{-1}$ [12]. Let us introduce an interaction whose strength decays as a power law with the exponent χ. The corresponding mobility matrix describing it is given by

$$\boldsymbol{O}_{nm} = \begin{cases} \boldsymbol{I}/\zeta & n = m \\ \frac{b^\chi}{\zeta|\boldsymbol{R}_n - \boldsymbol{R}_m|^\chi}\left[\boldsymbol{I} + \hat{\boldsymbol{r}}_{nm}\hat{\boldsymbol{r}}_{nm}\right] & n \neq m, \end{cases} \tag{A.24}$$

where $\hat{\boldsymbol{r}}_{nm}$ is a unit vector in the direction of $\boldsymbol{R}_n - \boldsymbol{R}_m$. For one dimension, the expression for $n \neq m$ is reduced to $\frac{b^\chi}{\zeta|\boldsymbol{R}_n - \boldsymbol{R}_m|^\chi}$. The generalized Langevin equation for the n-th monomer is written as:

$$\frac{\partial}{\partial t}\boldsymbol{R}_n = \sum_m \boldsymbol{O}_{nm}\left(-\frac{\partial U}{\partial \boldsymbol{R}_m} + \boldsymbol{f}_m(t)\right). \tag{A.25}$$

To solve this equation, we would need to simplify it. An approach previously taken by Kirkwood [29] for hydrodynamical interaction, was to approximate the mobility matrix by its average equilibrium value (this operation is call preaveraging). In our case, we can use the equilibrium distribution of the monomer-monomer distance Φ_{eq} to find the value of $\boldsymbol{O}_{nm}$ over all possible monomers realizations.

$$\boldsymbol{O}_{nm} \to \langle \boldsymbol{O}_{nm} \rangle = \int d\{\boldsymbol{R}_n\}\boldsymbol{O}_{nm}\Phi_{eq}\{\boldsymbol{R}_n\}. \tag{A.26}$$

To calculate it, we insert the distribution function (2.9). Since the distribution of $\hat{\boldsymbol{r}}_{nm}$ is independent of $|\boldsymbol{R}_n - \boldsymbol{R}_m|$, the average interaction can be written as

$$\langle \boldsymbol{O}_{nm} \rangle = \frac{b^\chi}{\zeta}\left\langle \frac{1}{|\boldsymbol{R}_n - \boldsymbol{R}_m|^\chi} \right\rangle \langle [\boldsymbol{I} + \hat{\boldsymbol{r}}_{nm}\hat{\boldsymbol{r}}_{nm}] \rangle \,. \tag{A.27}$$

Using $\langle \hat{\boldsymbol{r}}_{nm}\hat{\boldsymbol{r}}_{nm} \rangle = \frac{\boldsymbol{I}}{d}$, we have

$$\langle \boldsymbol{O}_{nm} \rangle = \frac{b^\chi \boldsymbol{I}\,(d+1)}{\zeta\, d}\left\langle \frac{1}{|\boldsymbol{R}_n - \boldsymbol{R}_m|} \right\rangle, \tag{A.28}$$

where d is the dimensionality.

$$\langle \boldsymbol{O}_{nm} \rangle = \int_0^\infty dr \frac{2\pi^{d/2}}{\Gamma\,(d/2)} r^{d-1}\left(\frac{d}{2\pi\,|n-m|\,b}\right)^{d/2} \exp\left(-\frac{dr^2}{2\,|n-m|\,b^2}\right)\frac{(d+1)\,b^\chi}{d\,\zeta r^\chi} =$$
$$= \frac{2\,(d+1)}{\Gamma\,(d/2)\;d}\left(\frac{d}{2\,|n-m|}\right)^{\chi/2}\frac{1}{\zeta}\int_0^\infty t^{d-1-\chi}\exp(-t^2)dt \equiv h\,(n-m)\,.$$

By using the relation

$$\int_0^\infty t^{d-1-\chi}\exp(-t^2)dt = \frac{1}{2}\Gamma(\frac{d-\chi}{2}), \tag{A.29}$$

Note that the integral converges only for $\chi < d$. We now find

$$h\left(n-m\right) = \frac{A_{d,\chi}}{\zeta\left|n-m\right|^{\chi/2}}, \tag{A.30}$$

where

$$A_{d,\chi} \equiv \frac{\Gamma(\frac{d-\chi}{2})\left(d+1\right)}{\Gamma\left(\frac{d}{2}\right)\ d}\left(\frac{d}{2}\right)^{\chi/2}. \tag{A.31}$$

We found the value of $\langle \boldsymbol{O}_{nm}\rangle$ in d dimensions. In fact, since in equilibrium the distance between monomers depends (up to a dimensionless factor) only on the distance along the chain $|n-m|$, any dimensional scaling disappears from the equation and the rest is embedded in the factor A.

Solving this equation requires transformation to the Fourier space

$$\frac{\partial}{\partial t}\boldsymbol{X}_p = \sum_q h_{pq}\left(-\kappa_q \boldsymbol{X}_q + \boldsymbol{f}_q(t)\right), \tag{A.32}$$

where κ_p is the same as in the Gaussian case and the mobility matrix:

$$h_{pq} = \frac{1}{N^2}\sum_{mn}\cos\left(n-1/2\right)\frac{p\pi}{N}\cos\left(m-1/2\right)\frac{q\pi}{N}h\left(n-m\right). \tag{A.33}$$

Changing from summation over the modes to integration, we find:

$$\begin{aligned} h_{pq} =& \frac{1}{N^2}\int_0^N dn\int_0^N dm\cos\left(\frac{p\pi n}{N}\right)\cos\left(m\frac{q\pi m}{N}\right)h\left(n-m\right) = \\ & \frac{1}{N^2}\int_0^N dn\Bigg[\cos\left(\frac{p\pi n}{N}\right)\cos\left(\frac{q\pi n}{N}\right)\int_{-n}^{N-n} dmh(m)\cos\left(\frac{q\pi m}{N}\right) \\ & -\cos\left(\frac{p\pi n}{N}\right)\sin\left(\frac{q\pi n}{N}\right)\int_{-n}^{N-n} dmh(m)\sin\left(\frac{q\pi m}{N}\right)\Bigg]. \end{aligned}$$

For large q values, we can replace the integration boundaries in the inner integrals with $\pm\infty$. The first inner integral can be approximated

$$\int_{-\infty}^{\infty} dmh(m)\cos(\frac{q\pi m}{N}) = \frac{A}{\zeta}\int_{-\infty}^{\infty} dm\frac{\cos(\frac{q\pi m}{N})}{|m|^{\chi/2}} = \frac{A}{\zeta}\left(\frac{N}{q\pi}\right)^{1-\chi/2}\int_{-\infty}^{\infty} dt\frac{\cos(t)}{|t|^{\chi/2}} = \frac{A}{\zeta}\left(\frac{N}{q\pi}\right)^{1-\chi/2} I$$

where I is the result of the integral in the last expression. Note that the integral I converges only for $0 < \chi < 2$. The second inner integral vanishes in the same approximation

$$\int_{-\infty}^{\infty} dm h(m) \sin(\frac{q\pi m}{N}) = 0.$$

Consequently,

$$h_{pq} \simeq \frac{AI}{N^2} \frac{N^{1-\chi/2}}{\zeta(q\pi)^{1-\chi/2}} \int_0^N dn \cos(\frac{p\pi n}{N}) \cos(\frac{q\pi n}{N}) = \frac{AI}{2N} \frac{N^{1-\chi/2}}{\zeta(q\pi)^{1-\chi/2}} \delta_{p,q}.$$

From this we find the dependence of the friction constant of a mode in q:

$$\zeta_q = (h_{qq})^{-1} = \frac{2(\pi)^{1-\chi/2}}{AI} N\zeta \left(\frac{q}{N}\right)^{1-\chi/2}. \tag{A.34}$$

Careful calculation of the h_{00}, gives us the friction constant for the center of mass

$$\zeta_0 = (h_{00})^{-1} = \frac{(2-\chi)(4-\chi)}{8A} \zeta N^{\chi/2}. \tag{A.35}$$

Remember that we already required $\chi < 2$ for the convergence of the integral I, so ζ_0 is always positive.

The friction coefficients are composed of q and N which scale with a χ dependent exponent, a dimensionless prefactor and ζ. The prefactor which depends on χ and d is the result of the transformation and integration. The scaling gives us the anomalous behavior of the system while the prefactor would only change rate of the motion, that is - will give us a χ dependent diffusion coefficient. Since we wanted to adhere to the convention of the Gaussian polymer, we choose to disregard the prefactor when writing our model equations.

A.5 Model

A.5.1 Model equations

In the previous section, we got a decoupled Langevin equation for every mode. The dynamical equations resulting from the addition of the interaction gave us the motivation for our model. We now define our model equation in the Rouse space as following:

$$\zeta_p \frac{\partial}{\partial t} \boldsymbol{X}_p = -\kappa_p \boldsymbol{X}_p(t) + \boldsymbol{W}_p(t), \tag{A.36}$$

where κ_q is the same as in Gaussian polymer. The noise mean and correlation are

$$\langle W_{p,\alpha}(t)\rangle = 0 \tag{A.37a}$$

$$\langle W_{p,\alpha}(t)\, W_{p',\beta}(t')\rangle = 2k_BT\zeta_p\delta_{p,p'}\delta_{\alpha,\beta}\delta(t-t'). \tag{A.37b}$$

And the friction coefficients are given by

$$\zeta_q = 2C_{\chi,N}N\zeta\left(\frac{q}{N}\right)^{1-\chi/2} \tag{A.38a}$$

$$\zeta_0 = \zeta N^{\chi/2}, \tag{A.38b}$$

where $C_{\chi,N}$ is a normalization factor of order unity. We explain its derivation in the next subsection.

A.5.2 Normalization of the dynamical equations of the model

In the Rouse model, the first mode friction coefficient ζ_1 differs by a factor of 2 from that of the center mass ζ_0. Thus, the slowest inner relaxation time is of the order of the time it takes for the polymer to diffuse its own radius of gyration. To adhere to this relation, we wanted our generalized model to have ζ_0 and ζ_1 of the same order. Since we have a freedom in choosing the normalization factor C, we choose it in such a way, that at very short times ($t \ll \tau_0$), when the mean square displacement of a monomer is $\langle \Delta R_n^2\rangle = 2D_0t$, the diffusion coefficient will be $D_0 = \frac{b^2}{\frac{1}{2}\frac{\zeta}{\kappa}}$. Under this condition, we derive an expression for C.

We begin from the Fourier transform definition (A.3b) and the expression for the time dependent variance of a mode (A.23). We write the expression for the mean square displacement of a monomer in terms of Rouse modes and develop in series for $t \ll \tau_0$:

$$\langle \Delta R_n^2\rangle = \left\langle (X_0(t)-X_0(0))^2\right\rangle + 4\sum_{p=1}^{N-1}\frac{k_BT}{\kappa_p}[1-\exp(-2t/\tau_p)] \approx$$

$$\left\langle (X_0(t)-X_0(0))^2\right\rangle + 4\sum_{p=1}^{N-1}\frac{k_BT}{\kappa_p}2t/\tau_p = \left\langle (X_0(t)-X_0(0))^2\right\rangle + \frac{4k_BTtN^{-\chi/2}}{C\zeta}\sum_{p=1}^{N-1}p^{\chi/2-1}.$$

Assuming we have $N = 2^l + 1$ monomers and our tagged monomer is $c = 2^{l-1}+1$, we

are left only with the even modes:

$$\langle \Delta R_c^2(t) \rangle = \frac{2k_BTt}{\zeta N^{\chi/2}} + \frac{4k_BTtN^{-\chi/2}}{C\zeta} \sum_{p=1}^{(N-1)/2} (2p)^{\chi/2-1} =$$

$$\frac{k_BTt}{\zeta} \left[\frac{2}{N^{\chi/2}} + \frac{2^{\chi/2+1}N^{-\chi/2}}{C} \sum_{p=1}^{(N-1)/2} (p)^{\chi/2-1} \right].$$

If we now insert our condition, we arrive to the expression

$$C = \frac{2^{\chi/2}N^{-\chi/2}}{1-N^{-\chi/2}} \sum_{p=1}^{(N-1)/2} (p)^{\chi/2-1}. \tag{A.39}$$

In the limit of large polymers ($N \gg 1$)

$$C = \frac{2}{\chi}. \tag{A.40}$$

For a Gaussian polymer ($\chi = 2$), we get $C = 1$ which is consistent with the definition of the Rouse equation for a Gaussian polymer.

Appendix B

Simulation methods

In our study we follow the location of a tagged monomer propagating according to our model (section 3.1.2). We do that by simulating equation (3.9) for each of the N independent modes. At each time step, we perform an inverse cosine transformation and find the location of the tagged monomer. We choose polymers of length $N = 2^l + 1$ where $l = 0, 1, 2, ...$ This choice was made for computational reasons. It can be easily shown that for such N the Fourier transform (equation (2.20b)) is reduced to the summation of the amplitude of the modes thus simplifying our calculations. To solve the equation numerically we use a derivative of the Metropolis Monte Carlo (MC) method.

The standard MC method [54, 55] is used to estimate the equilibrium or dynamical properties of a system with a certain Hamiltonian. It is based on stochastic Markov process, where a subsequent configuration of the system $\boldsymbol{A}'$ is generated from a previous configuration $\boldsymbol{A}$ with some transition probability $W(\boldsymbol{A}, \boldsymbol{A}')$. There are various methods to choose the elementary step. The transition probability is required to fulfill the *detailed balance principle* with the equilibrium distribution $P_{eq}\left(\overline{\boldsymbol{A}}\right)$:

$$P_{eq}\left(\overline{\boldsymbol{A}}\right) W(\boldsymbol{A}, \boldsymbol{A}') = P_{eq}\left(\overline{\boldsymbol{A}'}\right) W(\boldsymbol{A}', \boldsymbol{A}). \tag{B.1}$$

In the case of a simple RW, each configuration has the same weight, implying that the probability to select a motion $\boldsymbol{A} \rightarrow \boldsymbol{A}'$ is equal to that of the inverse transition $\boldsymbol{A}' \rightarrow \boldsymbol{A}$. If configuration $\boldsymbol{A}$ has energy $E(\boldsymbol{A})$, then at equilibrium, the probability of $\boldsymbol{A}$ is proportional to the Boltzmann weight $e^{-E(\boldsymbol{A})/k_BT}$ and hence (B.1) leads to requirement

$$\frac{W(\boldsymbol{A}, \boldsymbol{A}')}{W(\boldsymbol{A}', \boldsymbol{A})} = e^{-[E(\boldsymbol{A}')-E(\boldsymbol{A})]/k_BT}. \tag{B.2}$$

It is common to take the transition probability as the following

$$\begin{cases} W\left(\boldsymbol{A}, \boldsymbol{A}'\right) = e^{-[E(\boldsymbol{A}')-E(\boldsymbol{A})]/k_B T} & \text{, for } E\left(\boldsymbol{A}'\right) - E\left(\boldsymbol{A}\right) > 0 \\ W\left(\boldsymbol{A}, \boldsymbol{A}'\right) = 1 \quad \text{otherwise.} \end{cases} \tag{B.3}$$

At each time step, the algorithm changes configuration $\boldsymbol{A} \rightarrow \boldsymbol{A}'$. This can be an elementary step of a random walker for instance. The new configuration can be accepted or rejected. When the energy of the new configuration is smaller than that of the previous configuration, the new configuration is always accepted. If however the new configuration has higher energy, $\boldsymbol{A}'$ is accepted with a probability equal to the Boltzmann weight of the energy difference of the two configurations. Whether or not the configuration is accepted, the trial step is counted when calculating averages of the result - such as the mean time to get to a certain energy. When the number of iterations goes to infinity, the algorithm can reproduce the equilibrium distribution and all averages are guaranteed to reach their correct equilibrium value.

One of the shortcomings of the MC method is its slow convergence. Since the stepping mechanism is oblivious to the energy, steps to a new configuration with higher energy with respect to that of the current are as probable as steps to configurations with a lower one. As a result, many steps are discarded. We use a modification of the MC algorithm called Smart Monte Carlo (SMC) [56]. The difference lies in the stepping mechanism. At each iteration, the next step is calculated using an equation similar to the Langevin equation, only instead of a time derivative we find the step $\Delta \boldsymbol{r}$ through numerical integration with small time steps Δt

$$\Delta \boldsymbol{r} = \beta K \boldsymbol{F} + \boldsymbol{f}, \tag{B.4}$$

where $\boldsymbol{F}$ is the force, $\beta = 1/k_B T$, $\boldsymbol{f}$ is the Gaussian noise with distribution

$$Z(\boldsymbol{f}) = (4K\pi)^{-1/2} \exp(-\boldsymbol{f}^2/4K) \tag{B.5}$$

and $K \equiv \frac{\Delta t}{\zeta} = D\Delta t$. If K is chosen to be small enough, the trajectories generated by this equation are expected to provide accurate estimation for equilibrium averages. Usually in standard MC the direction of the step is chosen with equal probabilities up or down the potential slope. Here the step direction is biased by the direction of the force. The transition probabilities in SMC are also modified so that the equilibrium properties are

kept. It was shown numerically [56], that the averages of a system converge faster with the SMC method, than they did with standard MC.

Bibliography

[1] R. Metzler and J. Klafter. The random walk's guide to anomalous diffusion: a fractional dynamics approach. *Phys. Rep.*, 339:1, 2000.

[2] H. Scher and E.W. Montroll. Anomalous transit-time dispersion in amorphous solids. *Phys. Rev. B*, 12:2455, 1975.

[3] L.F. Richardson. Atmospheric diffusion shown on a distance-neighbour graph. *Proc. Roy. Soc.*, 110:709, 1926.

[4] P.-G. De Gennes. *Scaling Concepts in Polymer Physics*. Cornell University Press, Ithaca, 1979.

[5] M. Slutsky, M. Kardar, and L. A. Mirny. Diffusion in correlated random potentials, with applications to DNA. *Phys. Rev. E*, 69:061903, 2004.

[6] D. Brockmann and T. Geisel. Particle dispersion on rapidly folding random heteropolymers. *Phys. Rev. Lett.*, 91:048303, 2003.

[7] G. M. Viswanathan, V. Afanasyev, S. V. Buldyrev, E. J. Murphy, P. A. Prince, and H. E. Stanley. Lévy flight search patterns of wandering albatrosses. *Nature*, 381:413, 1996.

[8] G. Ramos-Fernández, J. Mateos, O. Miramontes, G. Cocho, H. Larralde, and B. Ayala-Orozco. Lévy walk patterns in the foraging movements of spider monkeys (ateles geoffroyi). *Behav. Ecol. Sociobiol.*, 55:223, 2004.

[9] J. Chuang, Y. Kantor, and M. Kardar. Anomalous dynamics of translocation. *Phys. Rev. E*, 65:011802, 2001.

[10] G. S. Grest and K. Kremer. Molecular dynamics simulation for polymers in the presence of a heat bath. *Phys. Rev. A*, 33:3628, 1986.

[11] K. Kremer and K. Binder. Dynamics of polymer chains confined into tubes: Scaling theory and Monte Carlo simulations. *J. Chem. Phys.*, 81:6381, 1984.

[12] M. Doi and S. F. Edwards. *The Theory of Polymer Dynamics (The International Series of Monographs on Physics)*. Oxford University Press, Oxford, 1988.

[13] W. Kuhn. Over the shape of threadlike molecules in solutions. *Kolloid*, 68:2, 1934.

[14] P.J. Flory. The configuration of real polymer chains. *J. Chem. Phys.*, 17:303, 1949.

[15] T. J. Murphy and J. L. Aguirre. Brownian motion of N interacting particles. i. extension of the Einstein diffusion relation to the N-particle case. *J. Chem. Phys.*, 57:2098, 1972.

[16] Prince E. Rouse. A theory of the linear viscoelastic properties of dilute solutions of coiling polymers. *J. Chem. Phys.*, 21:1272, 1953.

[17] H. Risken. *The Fokker-Planck Equation: Methods of Solutions and Applications*. Springer Series in Synergetics. Springer-Verlag, Berlin, 1996.

[18] B. H. Zimm. Dynamics of polymer molecules in dilute solution: Viscoelasticity, flow birefringence and dielectric loss. *J. Chem. Phys.*, 24:269, 1956.

[19] A. Klemm, H.-P. Müller, and R. Kimmich. NMR microscopy of pore-space backbones in rock, sponge, and sand in comparison with random percolation model objects. *Phys. Rev. E*, 55:4413, 1997.

[20] R. Kimmich. Strange kinetics, porous media, and NMR. *Chem. Phys.*, 284:253, 2001.

[21] W. D. Luedtke and U. Landman. Slip diffusion and Lévy flights of an adsorbed gold nanocluster. *Phys. Rev. Lett.*, 82:3835, 1999.

[22] O. V. Bychuk and B. O'Shaughnessy. Anomalous diffusion at liquid surfaces. *Phys. Rev. Lett.*, 74:1795, 1995.

[23] E. Fischer and R. Kimmich. NMR field gradient diffusometry of segment displacements in melts of entangled polymers. *J. Chem. Phys.*, 104:9174, 1996.

[24] M. Levandowsky, Benjamin S. W., and F. L. Schuster. Random movements of soil amebas. *Acta Pro. tozool.*, 36:237, 1997.

[25] R. Metzler and J. Klafter. The restaurant at the end of the random walk: recent developments in the description of anomalous transport by fractional dynamics. *J. Phys. A: Math. Gen.*, 37:R161, 2004.

[26] J. Klafter, A. Blumen, and M. F. Shlesinger. Stochastic pathway to anomalous diffusion. *Phys. Rev. A*, 35:3081, 1987.

[27] S. N. Majumdar and A. J. Bray. Spatial persistence of fluctuating interfaces. *Phys. Rev. Lett.*, 86:3700, 2001.

[28] T. Antal, M. Droz, G. Györgyi, and Z. Rácz. Roughness distributions for $1/f^{\alpha}$ signals. *Phys. Rev. E*, 65:046140, 2002.

[29] J. G. Kirkwood and J. Riseman. The intrinsic viscosities and diffusion constants of flexible macromolecules in solution. *J. Chem. Phys.*, 16:565, 1948.

[30] Y. Kantor and M. Kardar. Anomalous diffusion with absorbing boundary. *Phys. Rev. E*, 76:061121, 2007.

[31] L. Eugene. *Characteristic Functions*. Griffin, London, 1960.

[32] A. Zoia, A. Rosso, and M. Kardar. Fractional laplacian in bounded domains. *Phys. Rev. E*, 76:021116, 2007.

[33] S. Redner. *A guide to first-passage processes*. Cambridge University Press, Cambridge, 2001.

[34] S. Chandrasekhar. Stochastic problems in physics and astronomy. *Rev. Mod. Phys.*, 15:1, 1943.

[35] S. Nechaev, G. Oshanin, and A. Blumen. Anchoring of polymers by traps randomly placed on a line. *J. Stat. Phys.*, 98:281, 2000.

[36] S. B. Yuste and K. Lindenberg. Comment on "Mean first passage time for anomalous diffusion". *Phys. Rev. E*, 69:033101, 2004.

[37] M. Gitterman. Reply to "Comment on 'Mean first passage time for anomalous diffusion' ". *Phys. Rev. E*, 69:033102, 2004.

[38] G. Rangarajan and M. Ding. Anomalous diffusion and the first passage time problem. *Phys. Rev. E*, 62:120, 2000.

[39] A.V. Chechkin, R. Metzler, V.Y. Gonchar, J. Klafter, and L.V. Tanatarov. First passage and arrival time densities for Lévy flights and the failure of the method of images. *J. Phys. A: Math. Gen.*, 36:L537, 2003.

[40] R. Metzler and J. Klafter. Boundary value problems for fractional diffusion equations. *Physica A*, 278:107, 2000.

[41] G. Zumofen and J. Klafter. Absorbing boundary in one-dimensional anomalous transport. *Phys. Rev. E*, 51:2805, 1995.

[42] A. Bttcher and H. Widom. From Toeplitz eigenvalues through Greens kernels to higher-order Wirtinger Sobolev inequalities. *Oper. Theor.: Adv. Appl.*, 171:73, 2006.

[43] B. Dreiseikelmann. Translocation of DNA across bacterial membranes. *Microbiol. Mol. Biol. Rev.*, 58:293, 1994.

[44] D. Branton, J. J. Kasianowicz, E. Brandin, and D. W. Deamer. Characterization of individual polynucleotide molecules using a membrane channel. *Proc. Natl. Acad. Sci. USA*, 93:13770, 1996.

[45] M. Akeson, D. Branton, J. J. Kasianowicz, E. Brandin, and D. W. Deamer. Microsecond time-scale discrimination among polycytidylic acid, polyadenylic acid, and polyuridylic acid as homopolymers or as segments within single RNA molecules. *Biophys. J.*, 77:3227, 1999.

[46] W. Sung and P. J. Park. Polymer translocation through a pore in a membrane. *Phys. Rev. Lett.*, 77:783, 1996.

[47] D. K. Lubensky and D. R. Nelson. Driven polymer translocation through a narrow pore. *Biophys. J.*, 77:1824, 1999.

[48] K. W. Joanne, T. B. Gerard, and P. Debabrata. Passage times for unbiased polymer translocation through a narrow pore. *Phys. Rev. Lett.*, 96:208301, 2006.

[49] K. Luo, T. Ala-Nissila, S. Ying, P. Pomorski, and M. Karttunen. Comment on "Passage times for unbiased polymer translocation through a narrow pore", 2007.

[50] C. L. Rhonald and Y. G. Alexander. First passage times and asymmetry of DNA translocation. *Phys. Rev. E*, 72:061918, 2005.

[51] Y. Kantor and M. Kardar. Anomalous dynamics of forced translocation. *Phys. Rev. E*, 69:021806, 2004.

[52] C. Chatelain, Y. Kantor, and M. Kardar. Probability distributions for polymer translocation. *Phys. Rev. E*, 78:021129, 2008.

[53] N. Ahmed, T. Natarajan, and K.R. Rao. Discrete cosine transfom. *IEEE Trans. Comput.*, C-23:90, 1974.

[54] K. Binder and D.W. Heermann. *Monte Carlo Simulation in Statistical Physics: An Introduction*. Springer-Verlag, Berlin, 1997.

[55] C.P. Robert and G. Casella. *Monte Carlo Statistical Methods*. Springer-Verlag, Berlin, 1999.

[56] P. J. Rossky, J. D. Doll, and H. L. Friedman. Brownian dynamics as smart Monte Carlo simulation. *J. Chem. Phys.*, 69:4628, 1978.